UNIVERSITY OF BELGRADE

FACULTY OF BIOLOGY

Ahsein Addloli

STRUCTURAL AND REDOX REMODELING OF THE LIVER AND WHITE ADIPOSE TISSUE OF RATS IN METHIMAZOLE-INDUCED HYPOTHYROIDISM

Doctoral Dissertation

Belgrade, 2026

UNIVERZITET U BEOGRADU

BIOLOŠKI FAKULTET

Ahsein Addloli

STRUKTURNO I REDOKS REMODELIRANJE JETRE I BELOG MASNOG TKIVA PACOVA U HIPOTIROIDIZMU IZAZVANOM METIMAZOLOM

doktorska disertacija

Beograd, 2026

SUPERVISORS:

_____

Dr Aleksandra Korac, Full Professor

University of Belgrade-Faculty of Biology

_____

Dr Bato Korac, Senior Research Investigator

University of Belgrade-Institute for Biological Research „Sinisa Stankovic“-National Institute of Republic of Serbia

COMMITTEE MEMBERS:

_____

Dr Aleksandra Jankovic, Senior Research Investigator

University of Belgrade-Institute for Biological Research „Sinisa Stankovic“-National Institute of Republic of Serbia

_____

Dr Aleksandra Cvoro, Senior Research Investigator

University of Belgrade-Faculty of Biology

_____

Dr Marija Ilic, Research Associate

University of Belgrade-Faculty of Biology

BELGRADE,_____

ACKNOWLEDGEMENTS

The experimental work of the doctoral dissertation was done at the Institute of Zoology, Faculty of Biology, University of Belgrade, in cooperation with the Centre for Electron Microscopy, Faculty of Biology, University of Belgrade and at the Institute for Biological Research "Siniša Stanković"-National Institute of Republic of Serbia, University of Belgrade within the project: "White and/or brown: the importance of adipose tissue in maintaining the overall redox dependent metabolic control of physiological and metabolic adaptations" #173055, of the Ministry of Education, Science and Technological Development of the Republic of Serbia. The author was financially supported by the Libyan Ministry of Higher Education and Scientific Research.

This achievement would not have been possible without the support, guidance, and encouragement of many remarkable individuals, to whom I owe my deepest gratitude.

First and foremost, I would like to express my sincere and heartfelt appreciation to my supervisor, ***Prof. Aleksandra Korać,*** *for her exceptional guidance, unwavering support, and invaluable scientific insights throughout every stage of this research. I am truly honored to have had the opportunity to work under her supervision.*

I would also like to extend my deepest gratitude to ***Dr. Bato Korać,*** *for his generous support, insightful advice, and valuable recommendations throughout this journey.*

My sincere appreciation is also extended to the members of the doctoral examination committee each with his name and title for dedicating their valuable time to evaluate this dissertation. Their constructive comments, thoughtful suggestions, and professional evaluations have greatly improved the quality of this thesis, and I am truly grateful for their valuable contributions.

My deepest and most profound gratitude goes to my beloved family, and their continuous encouragement have been my greatest source of strength.

My special and heartfelt thanks are dedicated to my parents. No words can fully express my gratitude for their unconditional love, and this achievement belongs to them as much as it belongs to me. I dedicate this work to them with immense love, respect, and gratitude.

Finally, I thank everyone who contributed, directly or indirectly, to making this journey possible. I will always remain deeply grateful for your support and kindness.

Ahsein Mohamed. A. Addloli

STRUCTURAL AND REDOX REMODELING OF THE LIVER AND WHITE ADIPOSE TISSUE OF RATS IN METHIMAZOLE-INDUCED HYPOTHYROIDISM

SUMMARY

Thyroid hormones (TH) are key regulators of whole-body energy and metabolic homeostasis. However, the mechanisms by which TH deficiency affects lipid metabolism, peroxisomal dynamics, and redox regulation in metabolically active tissues remain unknown. Structural, organelle-specific, and redox remodeling in the liver and adipose tissue (AT) depots in methimazole-induced hypothyroid rats were investigated. Adult male Wistar rats received 0.04% methimazole for 7, 15, or 21 days and were compared with euthyroid controls. In the liver, hypothyroidism induced marked hepatocyte organelle remodeling accompanied by reorganization of antioxidant defense. Prolonged methimazole treatment reduced glutathione (GSH) content and glutathione peroxidase, glutathione reductase, and glutathione S-transferase activities, whereas thioredoxin reductase activity transiently increased after 7 and 15 days. Such changes (in antioxidant defence) indicate impaired GSH-dependent peroxide-removal capacity over time in hypothyroid liver. In white AT, methimazole induced depot-specific and time-dependent peroxisomal remodeling in subcutaneous, retroperitoneal, mesenteric, and gonadal depots. Coordinated but heterogeneous regulation of key peroxins (Pex11β, Pex19) and PPARα increased peroxisome abundance in white AT depots during hypothyroidism. Electron microscopy revealed distinct peroxisome biogenesis pathways and the emergence of pexopodium-like structures. ACOX1 immunolocalization showed that β-oxidation remained confined to peroxisomes, i.e., that pexopodia likely represent morphological adaptations associated with disturbed lipid metabolism in white AT. These findings provide new insight into liver- and white AT-specific redox remodeling and peroxisomal plasticity during hypothyroidism.

KEYWORD: liver, white adipose tissue, redox, hypothyroidism, remodeling

SPECIFIC FIELD: Biology

SPECIAL TOPICS: Cell and Tissue Biology

STRUKTURNO I REDOKS REMODELIRANJE JETRE I BELOG MASNOG TKIVA PACOVA U HIPOTIROIDIZMU IZAZVANOM METIMAZOLOM

SAŽETAK

Tiroidni hormoni (TH) su ključni regulatori energije celog tela i metaboličke homeostaze. Međutim, mehanizmi kojima nedostatak TH utiče na metabolizam lipida, peroksizomalnu dinamiku i redoks regulaciju u metabolički aktivnim tkivima i dalje su malo poznati. U disertaciji je ispitivano strukturno, specifično za organele, i redoks remodeliranje u jetri i depoima masnog tkiva (MT) kod pacova sa hipotiroidizmom izazvanim metimazolom. Odrasli mužjaci Wistar pacova pili su 0,04% rastvor metimazola tokom 7, 15 ili 21 dana i upoređeni su sa eutiroidnim kontrolama. U jetri, hipotiroidizam je izazvao izraženo remodeliranje organela hepatocita praćeno reorganizacijom antioksidativne odbrane. Produženi tretman metimazolom smanjio je sadržaj glutationa (GSH) i aktivnosti glutation peroksidaze, glutation reduktaze i glutation S-transferaze, dok se aktivnost tioredoksin reduktaze prolazno povećavala nakon 7 i 15 dana. Takve promene u antioksidativnoj odbrani jetre ukazuju na oštećen kapacitet uklanjanja peroksida koji je zavisan od GSH, tokom vremena uspostavljanja hipotiroidizma. Kod belog MT, metimazol je izazvao depo-specifično i vremenski zavisno peroksizomalno remodeliranje u potkožnim, retroperitonealnim, mezenteričnim i gonadalnim depoima. Koordinisana, ali heterogena regulacija ključnih peroksina (Pex11β, Pex19) i PPARα povećala je brojnost peroksizoma u depoima belog MT tokom hipotiroidizma. Elektronska mikroskopija je otkrila različite puteve biogeneze peroksizoma i pojavu struktura sličnih peksopodijumu. Imunolokalizacija ACOX1 je pokazala da β-oksidacija masnih kiselina ostaje ograničena na peroksizome, tj. da peksopodije verovatno predstavljaju morfološke adaptacije povezane sa izmenjenim metabolizmom lipida kod belog MT. Ovi rezultati pružaju novi uvid u redoks remodeliranje specifično za jetru i belo MT, kao i peroksizomalnu plastičnost tokom hipotiroidizma.

KLJUČNE REČI: jetra, belom masno tkivo, redoks, hipotiroidizam, remodeliranje

NAUČNA OBLAST: Biologija

UŽA NAUČNA OBLAST: Biologija ćelija i tkiva

TABLE OF CONTENTS

1. INTRODUCTION

1.1. LIVER

1.1.1. Structure and function of the rat liver

The liver is a one of the largest internal organs in mammals, and it is located in the upper right part of the abdomen. The liver of the rat is actualy multilobulated organ (Hebel and Stromberg, 1986). The mass of the rat liver accounts for about 6% of the total body weight (liver transverse diameter is 8.5–9.0 cm, weight is 15.5 g and respective volume is 22.6 ml) (Vdoviaková *et al.*, 2016).

It is enclosed by with a connective tissue capsule that extends into the interior, dividing the liver into lobes and obules (Figure 1A). The liver parenchyma is primarily composed of hepatocytes, organized into arrays of hepatic rows (Figure 1B).

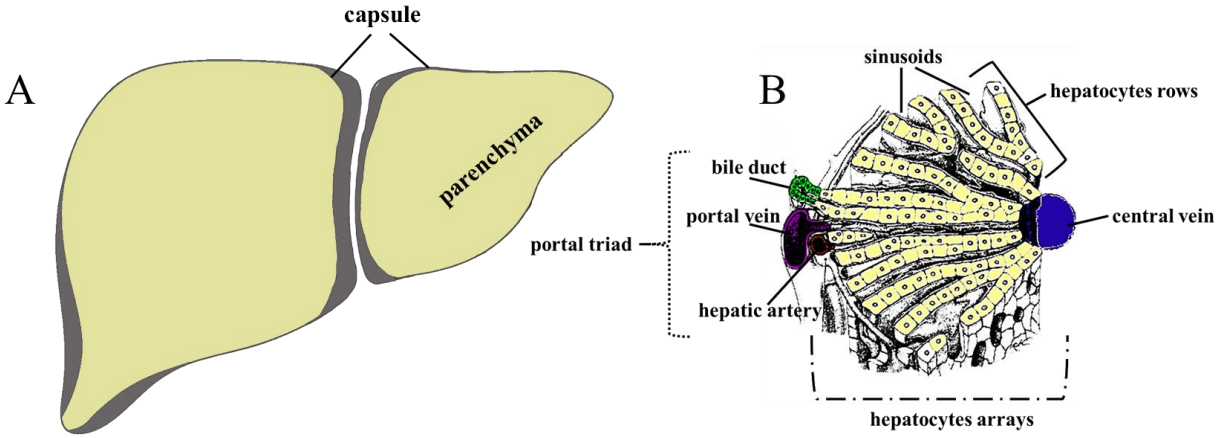

Figure 1. Schematic representation of rat liver anatomy and histology. Adopted and modify from Bloom and Fawcett, 1975.

Hepatic rows spread radially from the central vein to the periphery of the lobe where the portal triad (portal vein, hepatic artery and bile duct) is located. Between the rows there are long wide sinusoids (capillaries) (Figure 1B, 2). A network of reticular stroma made of collagen provides structural support to the hepatocytes and maintains the openness of the sinusoids within the lobules.

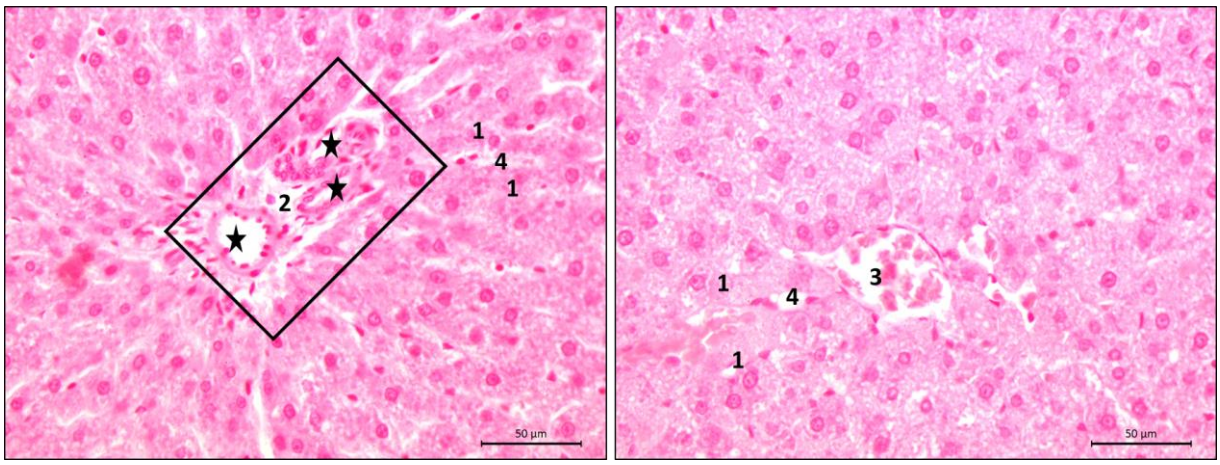

Figure 2. Histology of the rat liver. Paraffin sections stained with azocarmine. Hepatocytes (1) form one row radiating from portal tracts (2) to central veins (3), separated by sinusoids (4). Magnification: x40 orig., bar 50 µm.

The hepatic lobule, the basic structural unit, is hexagonal with a central vein at its core and portal triad at the vertices (Figures 3 and 4). By contrast, the hepatic acinus represents the functional unit,

defined by vascular supply and metabolic gradients. Acinar zones 1 (periportal) through 3 (pericentral) are assigned according to distance from the portal triad and decreasing oxygen tension.

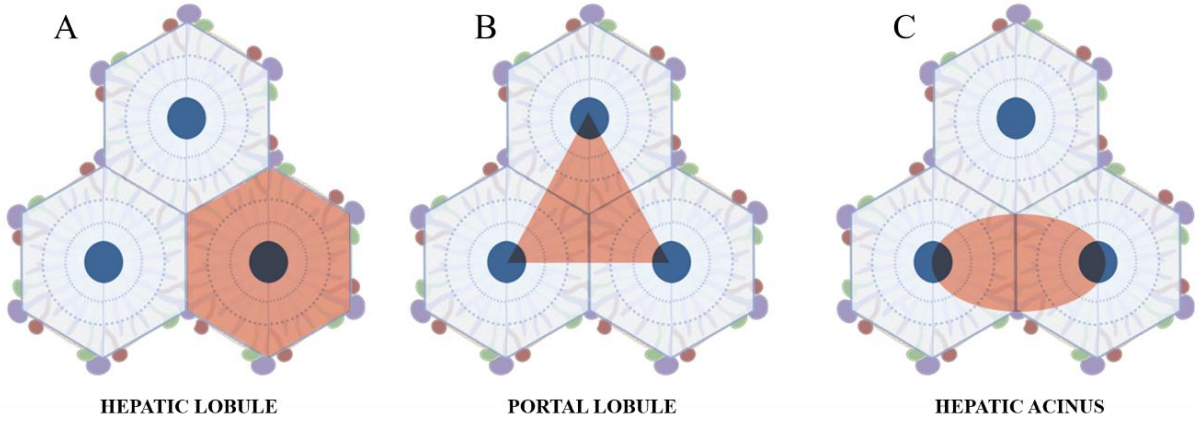

Figure 3. The hepatic lobular and acinar architecture (A-C). In the hepatic lobular model, the central vein (CV) is at the center of a lobule, while the portal tracts (PTs) are at the periphery. In contrast, in the acinar model hepatic acinus extend from CV of one hepatic lobule to the CV of the neighboring one.

The hepatocytes lined up in a sponge-like arrangement between the sinusoids along the portal-central axis show a remarkable heterogeneity with respect to their biochemical and physiological functions. Thus, hepatocytes possess dynamic structural and functional heterogeneity, recognized as metabolic zonation (Figure 4) (Gebhardt and Matz-Soja, 2014).

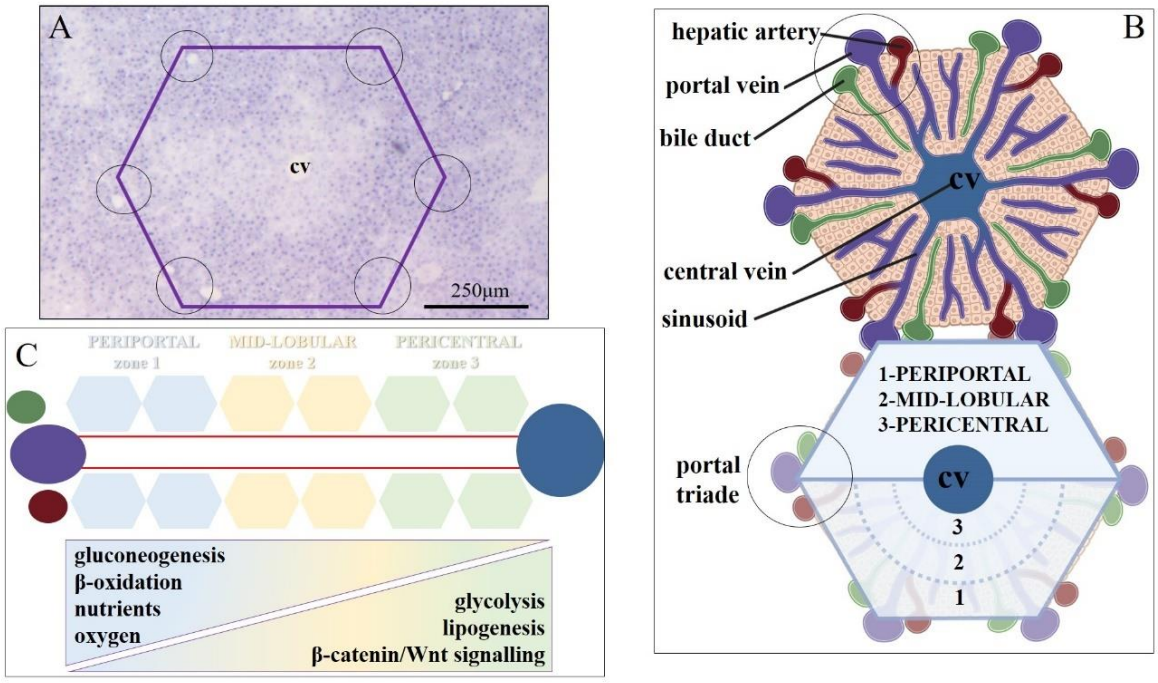

Figure 4. Hepatic lobular and acinar architecture (A, B), and their metabolic zonation (C). The hepatic acinus divides the hepatic parenchyma into three zones: zone 1 is closest to the blood supply, whereas zone 3 is the most distal. A-paraffin section of the rat liver stained with hematoxylin. Magnification: x5 orig., bar 250 µm.

The extracellular and cellular compartments of rat liver also show very different representations (Table 1). While extracellular compartments cover 15.7% of liver volume, the cellular compartment occupies 84.3%.

Table 1. Extracellular and cellular compartments of rat liver (data from Blouin *et al.*, 1977)

	Volume (%)	**Relative number of cells (%)**
Extracellular space compartment		
Sinusoidal lumen	10.6	
Disse space (perisinusoidal space)	4.7	
Biliary canaliculi	0.4	
Relative part of cells in total liver volume		
Hepatocytes	78	60
Non-hepatocytes	6.3	
Sinusoidal endothelial cells	2.8	19
Kupffer cells	2.1	15
Stellate cells (Ito)	1.4	6

In addition to hepatocytes, the liver also contains Kupffer cells (specialized macrophages), stellate (Ito) cells (responsible for storing fat and vitamin A) and endothelial cells of sinusoidal capillaries (Figure 5).

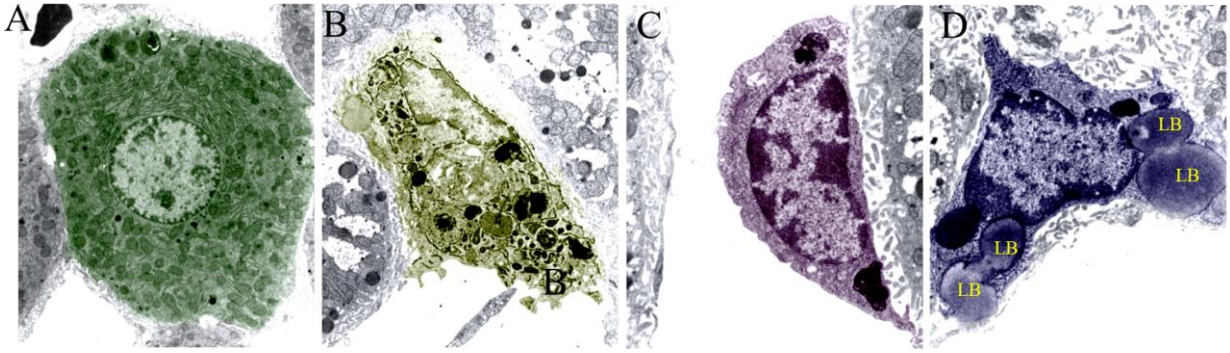

Figure 5. Electron micrographs various cell types in a rat liver. A) Hepatocyte; B) Kupffer cell; C) Endothelial cell; D) Fat-storing stellate cell (Ito). LB-lipid bodies. Magnification: A) x 3500; B) x 5000; C) x 9500 D) x 7500. Adopted and modified from Hollander *et al.*, 1985.

The main functions of the liver are the storage of nutrients and the elimination of harmful substances. It is considered the central laboratory of the organism since numerous anabolic and catabolic processes take place in it. The liver plays a major role in the metabolism of lipids and lipoproteins. A significant part of the free fatty acids absorbed in the digestive system reaches the liver, where they are oxidized or esterified into triacylglycerol (TG). The liver also produces lipids for all other tissues and organs in the form of lipoproteins. Apart from lipids, the liver is the main depot of glucose in the form of glycogen (Hollander *et al.*, 1985).

1.2 WHITE ADIPOSE TISSUE

1.2.1 Structure and function of rat white adipose tissue

White adipose tissue (white AT) in rats is organized into distinct anatomical depots divided into two classes: subcutaneous adipose tissue (SAT) and visceral adipose tissue (VAT) (Figure 6). Additionally, VAT consists of three main depots: gonadal, retroperitoneal and mesenteric (Figure XX). Gonadal VAT (gVAT) is the largest depot in males, situated near the testes; retroperitoneal

VAT (rVAT) is positioned deep in the abdominal cavity and closely associated with the kidneys, and mesenteric VAT (mVAT) is found along the digestive tract.

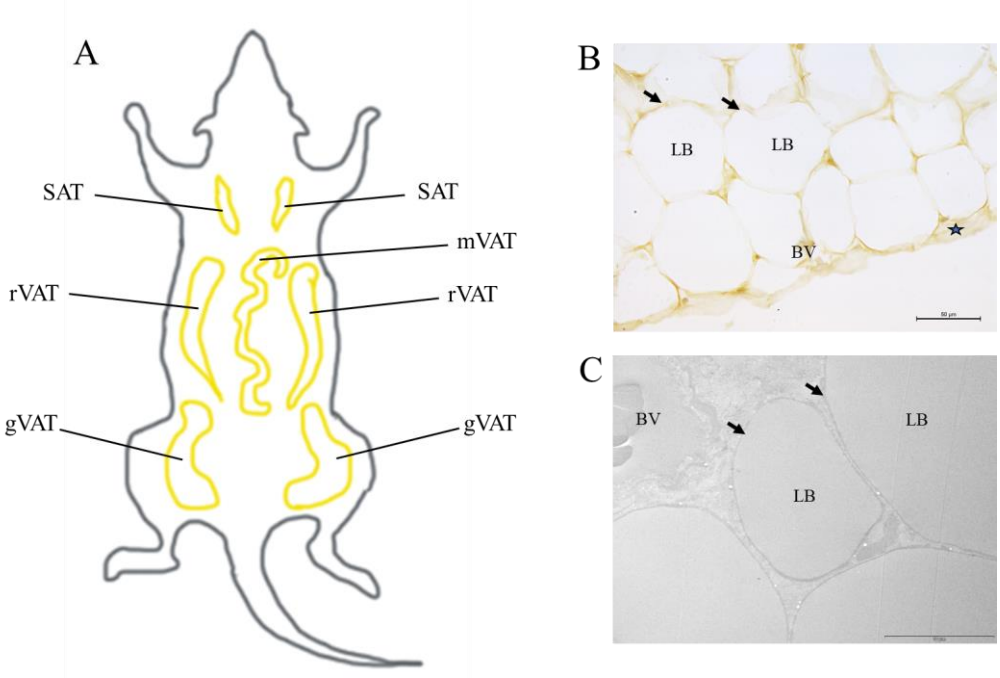

Figure 6. Anatomical location of major white adipose tissues in rats (A) and their appearance in light (B) and electron microscopy (C). White adipose tissues are mostly subcutaneous adipose tissue (SAT) and visceral adipose tissue (VAT). Major visceral depots in rodents include gonadal (gVAT), retroperitoneal (rVAT), and mesenteric (mWAT). Each depot has a lobular structure encapsulated with connective tissue. LB-lipid body; BV-blood vessel; arrow-white adipocyte cytoplasm; star-connective capsule. Magnification: x100, orig. bar 50 μm (A); x2650, orig. bar 10 μm (B).

Depots of SAT and VAT consist of numerous roundish white adipocytes filled with a single large lipid body surrounded by a thin cytoplasmic rim (Figure 6). A delicate connective tissue composed of reticular fibrils encircles the clusters of adipocytes.

The main functions of white adipocytes are energy storage and mobilisation (lipogenesis and lipolysis) and the production and secretion of various adipokines and cytokines. In addition, white AT serves as a thermal insulator and mechanical protector (Trayhurn and Beattie, 2001).

1.3 Thyroid hormones, lipid metabolism, and hypothyroidism

Thyroid hormones (TH) influence nearly all major metabolic pathways. Their most prominent role is increasing basal energy expenditure by regulating the metabolism of proteins, carbohydrates, and lipids (Pucci *et al.*, 2000). In this way TH influences energy metabolism and storage in adipose tissue, as well as fatty acid metabolism and transport in the liver. Thyroid hormones stimulate the utilization of lipid substrates owing to the increased mobilization of triacylglicerole stored in adipose tissue. It is also known that thyroid hormone can regulate hepatic metabolic pathways including cholesterol metabolism, *de novo* lipogenesis, fatty acid oxidation, as well as carbohydrate metabolism (Sinha *et al.*, 2018).

Dysregulation of TH levels, as seen in hypothyroidism, has been associated with dyslipidemia and metabolic dysfunction-associated fatty liver disease (Soares De Oliveira and Ritter, 2024). However, the link between white AT hypertrophy (obesity) or higher body mass index and liver steatosis and fibrosis in hypothyroidism has been firmly established (Lazo-de-la-Vega-Monroy *et al.*, 2023; Ayati Firoozabadi *et al.*, 2025). Hypothyroidism is associated with numerous metabolic disorders, primarily with disorders of lipid metabolism (Mason *et al.*, 1930). It has been shown in the

literature to cause an increase in total cholesterol, low-density lipoprotein (LDL) cholesterol, apolipoprotein B, and lipoproteins in the serum of patients (Pearce, 2012). Hypothyroidism also affects carbohydrate metabolism in the liver, as well as glucose turnover in peripheral tissues, skeletal muscle, and adipose tissue. Due to the numerous disorders it causes, hypothyroidism has been recognized as one of the risk factors for the development of nonalcoholic fatty liver disease (NAFLD) associated with hyperlipidemia, obesity, and insulin resistance (Chung *et al.*, 2012).

1.4 Experimental models of hypothyroidism

In adult animals, the induction of hypothyroidism can be achived using methimazole (1-methyl-2-mercaptoimidazole) (Čakić-Milošević *et al.*, 2004; Aleksic *et al.*, 2021).

Methimazole, which is used in the treatment of hyperthyroidism in humans (Cooper, 1984), inhibits the biosynthesis of thyroid hormones by acting as a false substrate for peroxidase, preventing further iodination of tyrosine residues in thyroglobulin (Figure 7).

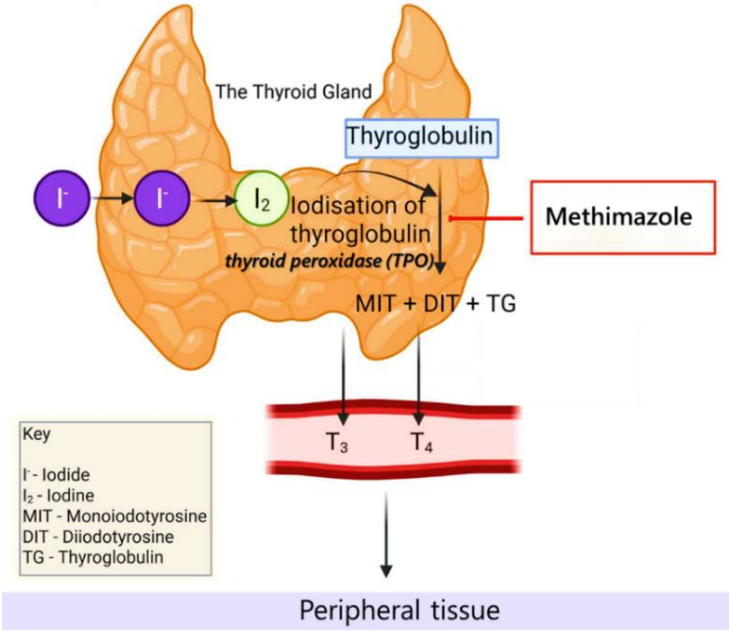

Figure 7. Methimazole mechanism of action. In thyroid gland methimazole reduces thyroid hormone production primarily by inhibiting thyroid peroxidase (TPO), the key enzyme responsible for synthesizing T_3 and T_4. By blocking TPO, it prevents the oxidation of iodide and its incorporation into thyroglobulin (iodination), as well as the subsequent coupling of iodotyrosine residues (Cooper, 1984). Inhibition of thyroid function is achieved after 2-4 weeks (until depletion of the stored thyroxine in the colloid).

Methimazole is absorbed through the mucosa of the small intestine, reaching peak plasma concentrations one to two hours after ingestion, and is concentrated in the thyroid gland. The half-life of methimazole is 4–6 hours, after which it is metabolized in the liver, and its metabolites and part of the unchanged drug are excreted in the urine (Rollins and Blumenthal, 2016). Methimazole, unlike propylthiouracil, exerts its effect exclusively in the thyroid gland, does not block deiodinase in peripheral tissues, thus making the hypothyroid state systemic rather than local.

1.5 Hypothyroidism and reactive oxigen species (ROS)

Thyroid hormones play an important role in the regulating of the metabolism in all cells and tissues (Seifert *et al.*, 2023). Substantial data in the literature show that the effects of thyroid hormones on cellular metabolism are closely linked to regulating ROS production. Since the general metabolic

effect of thyroid hormones is a relative acceleration of the basal metabolism, it has been expected that hyperthyroidism is coupled with an increase in oxidative pressure and cellular damage (Kochman *et al.*, 2021), while hypothyroidism causes a hypometabolic state associated with metabolic dysfunction (Tanase *et al.*, 2020; Wang *et al.*, 2024; Yorke, 2024) and decreased oxidative pressure (Oren *et al.*, 1996). However, published data on the effects of hypo- and hyperthyroidism on ROS production and antioxidant defense organization in many tissues are quite inconsistent. For example, hypothyroidism has no effect on (Venditti *et al.*, 1997), reduces (da Rosa Araujo *et al.*, 2010) or increases (Sahoo *et al.*, 2008; Gariani and Jornayvaz, 2021) oxidative damage in metabolically active organs. It seems likely that several factors determine the outcomes of hypothyroidism, including the strategy for its induction (chemical or surgical thyroidectomy) and, in the case of chemical induction, the route of drug administration, the dose used, and the length of treatment. Furthermore, data show that hypothyroidism also compromises mitochondrial function, resulting in ATP depletion, membrane depolarization, and excessive ROS production (Baskol *et al*., 2007; Ramanathan *et al.*, 2023).

The primary defense in tissues against ROS is the antioxidant defense. Antioxidant defense comprises both enzymatic and nonenzymatic components that are essential for maintaining tissue redox homeostasis and protecting against harmful effects of ROS in virtually all cells of aerobic organisms (Jomova *et al.*, 2023). Generally, the main components of antioxidant defense include superoxide dismutase enzymes – such as copper, zinc superoxide dismutase (CuZnSOD, EC 1.15.1.1) and manganese superoxide dismutase (MnSOD, EC 1.15.1.1) as well as other enzymatic and nonenzymatic components that cooperate in regulating peroxide levels, like catalase (EC 1.11.1.6), glutathione (GSH), glutathione peroxidase (GSH-Px, EC 1.11.1.9), glutathione reductase (GR, EC 1.6.4.2), as well as thioredoxin (Trx) and thioredoxin reductase (TR, EC 1.8.1.9). Organization of antioxidant defense is tissue-specific and susceptible to alterations in response to changes in oxidative pressure and tissue metabolic activity (Buzadžić *et al.*, 2007; Jankovic *et al.*, 2009).

1.6 The effects of hypothyroidism on the liver and white adipose tissue

The liver and white adipose tissue act together in the lipogenic/lipolytic axis that balances the production, distribution, and storage of lipids. The impact of hypothyroidism on hepatocytes and white adipocytes has been studied at metabolic and physiological levels, but little is known about its effects on the structural and redox remodeling of these cells and tissues (Venditti *et al.*, 1997). Furthermore, data in the literature regarding the impact of hypothyroidism on the liver and other organs are contradictory (Cano-Europa *et al.*, 2010, 2011*)*, whereas very little is known about its impact on white adipose tissue.

The epidemic of obesity in the human population and the metabolic syndrome associated with it represent a pressing medical problem. Given that thyroid hormones are most closely associated with oxidative and synthetic processes in the lipogenic/lipolytic axis, their deficiency is expected to lead to metabolic silencing of the tissue. But does this also lead to tissue and cellular silencing in terms of organelle reduction and/or redistribution? Does it affect antioxidant defense enzymes and redox-regulated processes of structural remodeling of the liver into white adipose tissue? These are some of the questions this doctoral dissertation will answer, which will also represent its scientific contribution.

2. AIMS

The upsurge in hypothyroidism as a metabolic disease, especially among young people, is worrying. in euthyroidism of unknown etiology. There are several known causes – such as congenital disorders of hormone synthesis and side effects from methimazole treatment for hyperthyroidism – as well as the insidious development of metabolic and hormonal imbalances in otherwise euthyroid patients of unknown etiology.

However, the molecular basis of the establishment of hypothyroidism at the level of the liver and white adipose tissue, which are associated with lipid metabolism is insufficient. Given that hypothyroidism has a direct impact on lipid metabolism, it is important to reveal the underlying structural and redox changes. Given that the liver and white adipose tissue constitute the main lipogenic/lipolytic axis and thus the main reservoir of lipids in the body, and that hypothyroidism disrupts this balance, the aims of the doctoral dissertation are:

1. Investigating the impact of hypothyroidism on the structural remodeling of the liver and white adipose tissue depots;

2. Exploring the biogenesis of hepatocyte and adipocyte organelles, specifically lipid bodies and peroxisomes;

3. Investigating the redox mechanisms underlying tissue, cell, and organelle remodeling.

3. MATERIAL AND METHODS

3.1 Experimental design

3.1.1 Animals and treatments

The research was performed on tissue and organ archived samples collected from an experiment approved by the Ministry of Agriculture and Environmental Protection - Veterinary Administration (No. 323-07-07505/2015-05/4 of 26.11.2015 and No. 323-07-06857/2011-05 of 17.09.2021) for the welfare of animals and to prevent their excessive and unethical use in experimental research. Male Wistar rats, two months old, were used in the experiment. The animals were divided into four groups (each consisting of 8 animals), of which three groups were given a 0.04% methimazole solution in tap water for 7, 15 or 21 days (M7, M15 and M21 group respectively), and the fourth was a control-euthyroid group, given tap water. All animals were sacrificed on the same day by decapitation, and the liver and subcutaneous white AT (SAT) and visceral AT (VAT) depots (gonadal – gVAT, retroperitoneal – rVAT, mesenteric – mVAT), were isolated and prepared according to routine protocols for tissue preparation for light and electron microscopy, immunohistochemistry and protein expression analysis, as well as for enzyme activity determination.

3.2 Preparation of the tissue for analysis

3.2.1 Preparation of the tissue for light microscopy

Immediately after isolation, a portion of liver and adipose tissue depots was fixed for light microscopy in 4% paraformaldehyde in phosphate buffer (pH 7.4). After fixation, samples were rinsed in tap water overnight, then passed through a series of increasing concentrations of ethanol for dehydration, xylene-cleared, and finally embedded in paraffin. Paraffin sections of 5 μm were stained with hematoxylin, AZAN trichrome, periodic acid and Shiff (PAS), and also used for immunohistochemical and immunofluorescent detection of catalase.

3.2.2 Preparation of the tissue for transmission electron microscopy

Small parts of SAT and VAT depots (mVAT, rVAt and gVAT) immediately after dissection were fixed with 2% glutaraldehyde/2% paraformaldehyde in 0.1 M Sørensen phosphate buffer (PB), pH 7.2 for 1h at 4°C. After fixation, tissue was rinsed in PB and then preincubated in 0,1% 3, 3'-diaminobenzidine (DAB) in PB for 30 minutes, for peroxidase staining (LeHir *et al.*, 1979). Then, 0.01% H2O2 was added to the preincubation medium and incubated for 1h at 37°C. After rinsing in PB, tissue was postfixed in 2% osmium tetroxide in the same buffer, then routinely dehydrated and embedded in Araldite.

Other portions of the same SAT and VAT depot samples as well liver were routinely fixed in 2.5% glutaraldehyde in 0.1 M Sørensen PB for 1h at 4°C, postfixed in 2% osmium tetroxide in the same buffer, and routinely dehydrated and embedded in Araldite. Semi-thin sections of 2 μm were obtained using a Leica UC6 ultramicrotome (Leica Microsystems, Wetzlar, Germany), transferred to microscope slides, stained with toluidine blue for light microscopy analysis and orientation for ultrastructural sectioning. Ultra-thin sections (80-100 nm) of white AT depots and liver were mounted on copper or nickel grids and examined on a Philips CM12 transmission electron microscope (Philips/FEI, Eindhoven, The Netherlands) equipped with the digital camera SIS MegaView III (Olympus Soft Imaging Solutions, Münster, Germany). The obtained electron micrographs were used for morphological/stereological analyses.

3.2.3 Preparation of the tissue for Western blotting

After decapitation, the right portion (rVAT, gVAT) or half portion (SAT, mVAT, liver) of tissues was frozen immediately. Tissues were prepared in sucrose buffer for Western blot (adipose tissue depots) and enzyme activity (adipose tissue depots and liver) analyses. Protein concentration from tissue samples was determined spectrophotometrically according to the method based on the biuretic reaction of peptide bonds from proteins with copper (Cu) in an alkaline environment (Lowry *et al.*, 1951). The resulting Cu^{+} ion further reacts with Folin's reagent- the Folin-Ciocalteau reaction, based on the reduction of phosphomolybdotungstenate to heteropolymolybdenum blue, due to the copper-catalyzed oxidation of aromatic amino acids. As a result, a blue-colored complex is formed whose absorption maximum is at 500 nm. The absorbance of the samples at 500 nm was read on a UV-VIS spectrophotometer (UV-1900i Shimadzu). The protein concentration in the sample is proportional to the intensity of the color, that is, the presence of aromatic amino acids in the proteins. To read the protein concentration in the samples, the linear part of the standard curve is used, which is formed by measuring the absorbance of albumin solutions of increasing and known concentrations. The sensitivity of this method is 0.01 mg/mL of protein, and the concentration of total proteins is expressed in mg/mL.

3.3 SDS-PAGE and Western blot

3.3.1 Protein electrophoresis

On the basis of molecular masses, proteins were separated by sodium dodecyl sulfate (SDS)-polyacrylamide electrophoresis (SDS-PAGE) in the Mini-Protean III system (BioRad). Protein separation gels differed in acrylamide (AA) concentration, depending on the molecular weight of the target protein, while concentrating gels were always 5% (5% AA, 0.1% SDS, 0.125 M Tris, pH 6.8). Polymerization of the gels was enabled by adding 0.05% ammonium persulfate and 0.033% N,N,N′,N′-tetramethyl-ethylenediamine (TEMED). The separation buffer contained 0.192 M glycine, 0.1% SDS, and 0.025 M Tris, pH 8.3. Protein samples of a specified volume were mixed with the same volume of sample buffer (4% SDS, 20% glycerol, 10% β-mercaptoethanol, 0.025% bromo-phenol blue, 0.125 M Tris, pH 6.8) before loading on the gel, and then denatured by boiling for 5 min. at 95 °C. Depending on the target protein, 5-20 μg of protein from the sample was applied. A protein marker (BioRad) was also applied to the gels to determine the molecular masses. Electrophoresis lasted 90-120 min. at a discontinuous current intensity and a constant voltage of 100 V. After transferring the protein to the separation gel, the voltage was increased to 120 V. After electrophoresis, the gels were further used for Western blot analysis.

3.3.2 Protein transfer from SDS-polyacrylamide gel to membrane and immunological detection of immobilized proteins (Western blot)

Proteins were transferred from the gels by wet electrotransfer to polyvinyl difluoride (PVDF) membranes (Amersham Hybond P 0.45 μm). Membranes were previously activated in methanol (10 seconds) and distilled water (3 minutes). Protein transfer from gels to membranes took place at a constant voltage of 100 V, 60 min. in transfer buffer (0.192 M glycine, 20% methanol, 0.025 M Tris, pH 8.3). Transfer success was checked with a 5% solution of Ponceau S dye in glacial acetic acid. Membranes were then destained by rinsing in Tris buffer supplemented with Tween 20 (0.2 M Tris, 1.5 M NaCl, 0.05% Tween 20, pH 7.4) and incubated for 60 min. at room temperature in serum for blocking free sites on the membrane - 5% BSA (eng. Bovine serum albumin) in Tris buffer with the addition of Tween 20. After blocking, the membranes were incubated with the primary antibody dissolved in 5% BSA overnight at 4 °C. Data on the antibodies used in this experiment are shown in

Table 1. After rinsing off the excess of the primary antibody, the membranes were incubated with the corresponding secondary antibody obtained by immunization of goat against rabbit IgG, i.e. mouse (Goat-anti rabbit HRP, Abcam and Goat-anti mouse HRP, Abcam), in a dilution of 1:15000, i.e. 1:4000 in 5% BSA for 2 h at room temperature. After incubation, the membranes were rinsed with Tris buffer with the addition of Tween 20 detergent, for 30 minutes at room temperature. For protein visualization, the membranes were incubated for 3 minutes in a chemiluminescent substrate - luminol, with the addition of H2O2. After incubation in luminol, the signal from the membranes was scanned using an iBright CL750 Imaging System (Thermo Fisher Scientific). The obtained images were further used for the quantification of protein bands.

Table 1. Primary antibodies used for Western blot analysis.

Antibody	Dilution	Manufacturer	Catalog number
peroxisomal biogenesis factor 11β (Pex11β)	1:1000	Abcam (Cambridge, UK)	ab74507
peroxisomal biogenesis factor 19 (Pex19)	1:2000	Abcam (Cambridge, UK)	ab137072
peroxisome proliferator-activated receptor alpha (PPARα)	1:2000	Abcam (Cambridge, UK)	ab8934
β-actin	1:2000	Abcam (Cambridge, UK)	ab8226

3.3.3 Quantification of results obtained by Western blot analysis

Densitometric analysis of the obtained protein bands was performed using the ImageJ software package. The darkening intensity (eng. volume) of the circled strip is represented as the sum of all pixel values excited by the signal (1 pixel = 0.007744 mm2) within the strip minus the background. The values obtained for the target proteins were normalized in relation to the values obtained for GAPDH or β-actin as a constitutively expressed protein e.g. housekeeping protein.

3.4 Analysis of antioxidant defense enzyme activity and total GSH content

3.4.1 Analysis of catalase enzyme activity

Catalase activity was determined by the Beutler method (Beutler, 1982), which involves spectrophotometric monitoring of the change in H_2O_2 absorbance that changes due to the decomposition of a standard concentration of H_2O_2 (10 mM) by catalase from the sample. The change in absorbance is monitored at 230 nm wavelength because H_2O_2 has the absorption maximum there. Catalase activity was calculated using the molar extinction coefficient for H_2O_2 (0.071), and the final values were expressed in units of catalase activity per mg of protein.

3.4.2 Analysis of glutathione peroxidase enzyme activity

GSH-Px enzyme activity was determined according to the method of Paglia and Valentine (1967), which is based on spectrophotometric monitoring of the change in NADPH absorbance at 340 nm wavelength due to its oxidation. NADPH is used to reduce oxidized glutathione (GSSG) by glutathione reductase, and then GSSG is recycled from reduced glutathione (GSH) by GSH-Px. GSH-Px activity is expressed in units per mg of protein, and a unit of GSH-Px activity is defined as 1 nM NADPH oxidized per minute.

3.4.3 Analysis of glutathione S-*transferase enzyme activity*

GST enzyme activity was determined according to the method of Habig *et al.* (1974). GST catalyzes the conjugation reaction of 1-chloro-2,4-dinitrobenzene (CDNB) with the thiol (-SH) group of glutathione, resulting in a CDNB-glutathione conjugate. Enzyme activity was determined by measuring the change in absorbance of the resulting conjugate at 340 nm. GST activity was calculated using the molar extinction coefficient for CDNB (9.6), and the final values were expressed in nM GSH min^{-1} mg^{-1} protein.

3.4.4 Analysis of glutathione reductase enzyme activity

GR enzyme activity was determined according to the method of Glatzle *et al.* (1974), which is based on spectrophotometric monitoring of NADPH oxidation at 340 nm wavelength. NADPH is oxidized during the reduction of oxidized glutathione (GSSG) in a reaction catalyzed by GR. GR activity is expressed in units per mg of protein, and a unit of GR activity is defined as 1 nM NADPH oxidized per minute.

3.4.5 Analysis of thioredoxin reductase enzyme activity

TR enzyme activity was determined according to the method of Luthman and Holmgren (1982). TR catalyzes the reduction of the disulfide bond in 5,5′-dithio-bis(2-nitrobenzoic acid) (DTNB) to trinitrobenzene (TNB), with NADPH as a cofactor. This reaction is monitored through the oxidation of NADPH spectrophotometrically as an increase in absorbance at a wavelength of 412 nm during the first two minutes of the reaction. TR activity is expressed in units per mg of protein, and a unit of TR activity is defined as nM NADPH oxidized per minute.

3.4.6 Analysis of superoxide dismutase enzyme activity

The activity of SOD isoforms (MnSOD and CuZnSOD) was determined according to the modified method of Misra and Fridovich (1972). This method is based on the ability of SOD to inhibit the autoxidation of adrenaline to adrenochrome in a basic environment, releasing superoxide anion radicals that accelerate this reaction. The speed of autoxidation of adrenaline is monitored spectrophotometrically at a wavelength of 480 nm, and the measure of enzyme activity is the degree of inhibition of the reaction. A unit of SOD activity is defined as the amount of protein that leads to 50% inhibition of the autoxidation rate of adrenaline in the linear part of the absorbance change. SOD activity is expressed in units per milligram of protein.

3.4.7 Analysis of total glutathione content

The amount of total glutathione (reduced, GSH and oxidized, GSSG) was determined in the tissue according to the method of Griffith (1980), after protein precipitation in the sample with 10% sulfosalicylic acid. The method is based on the oxidation of reduced glutathione (GSH) by 5,5'-dithio-bis-(2-nitrobenzoic acid) (DTNB), whereby 5-thio-2-nitrobenzoic acid (TNB) and oxidized glutathione (GSSG) are formed. TNB is a yellow compound with an absorption maximum at 412 nm and its rate of formation is proportional to the concentration of GSH in the sample, which can be determined by measuring the change in absorbance at 412 nm. GR catalyzes the reduction of the resulting GSSG to 2 GSH in the presence of NADPH, and GSH then reacts again with DTNB to form TNB. The measured amount of glutathione in the sample represents the sum of reduced and oxidized glutathione ([GSH]total = [GSH] + 2 x [GSSG]). The amount of glutathione in the samples is calculated based on the linear part of the previously prepared standard curve of different concentrations of GSH, and is expressed in nM GSH min^{-1} g^{-1} tissue.

3.5 Analysis of protein localization by microscopic methods

3.5.1 Immunohistochemical protein localization

Immunohistochemical analysis for the detection of protein expression and localization was performed on paraffine sections with a thickness of 5 μm. Sections were previously put through the routine process of deparaffinisation and rehydration. Then, the sections were incubated for 10 min in 10 mM citrate buffer (pH 6.0) at 600 W in the microwave and rinsed with TBS buffer to reveal epitopes, i.e. antigen binding sites. ABC kit (Abcam) was used for immunodetection of proteins in streptavidin-biotin-peroxidase samples according to the manufacturer's protocol. Non-specific antibody binding sites were blocked by incubating the sections in Protein Block albumin solution (Abcam) at room temperature for 30 minutes. Sections were incubated overnight at 4 °C with primary antibody against catalase (ab1877, 1:1000). Sections were then rinsed in Tris buffer with added Tween 20 detergent and incubated for 10 min. at room temperature with appropriate secondary anti-mouse or anti-rabbit antibodies (1/20) for 2 hours at room temperature. After incubation and rinsing again, sections were incubated with peroxidase-conjugated streptavidin at room temperature for 10 min.

Binding sites of primary antibodies to target proteins on tissue sections were detected by incubation with 0.05% 3,3′-diaminobenzidine (DAB) (DAB kit, Agilent Technologies, Santa Clara, CA, USA) in the presence of 0.012% H_2O_2, in the dark until the reaction occurred. The development of the color reaction was stopped by rinsing with tap water, and the sections were then counterstained with hematoxylin. After routine dehydration through a series of increasing concentrations of ethanol, permanent preparations were made by mounting the sections in DPX medium (distyrene and xylene; Sigma-Aldrich). The samples were further analyzed on a DMLB light microscope equipped with a DFC295 digital micrograph camera (Leica Microsystems). To determine antibody specificity, control sections without incubation with primary or secondary antibodies were also analyzed immunohistochemically.

3.5.2 Immunofluorescent protein localization

Patterns of cellular localization of target proteins in liver tissue was analyzed by confocal microscopy. After antigen retrieval and rinsing in TBS buffer, serial 5-μm-thick paraffin sections were incubated in 10% normal goat serum and 1% BSA in TBS supplemented with Tween 20 at room temperature for 60 min to block nonspecific antibody binding sites. Sections were then incubated overnight with the primary antibodies against catalase (ab1877, 1:1000) at 4 ºC. After rinsing, sections were incubated with appropriate fluorochrome-conjugated secondary antibodies at room temperature for 60 min in the dark (Alexa Fluor® 633 goat anti-rabbit, Life Technologies). After two rinses in TBS buffer supplemented with Tween 20 detergent, and one in TBS, sections were incubated for 5 min with the fluorescent dye Sytox Orange (S11368, 1/1000, Thermo Fisher Scientific) to contrast nuclei. After rinsing again in TBS, Mowiol (Polysciences) was used as mounting medium. Depending on the origin of the primary antibodies, two methods were used: the double simultaneous immunofluorescence method (if the primary antibodies originate from different hosts) and the double sequential immunofluorescence method (if the primary antibodies originate from the same host). The samples were further analysed using a Leica TCS SP5 II confocal microscope (Leica Microsystems) and LAS-AF (LAS-AF-Lite 2.6.3 8173) software.

3.5.3 Immunogold labeling

Ultra-thin sections of white AT depots routinely prepared for electron microscopy examination were obtained using a Leica UC6 ultramicrotome (Leica Microsystems, Wetzlar,

Germany) and mounted on nickel grids. After antigen retrieval in 10mM citrate buffer and incubation with 5% BSA in Tris-buffered saline/0.1% Tween 20 (TBS-T) for 1h at room temperature, grids were incubated overnight at 4°C with primary anti-ACOX1 (acyl-CoA oxidase 1) antibody (1:50, ab184032) or anti-catalase antibody (1:50, ab1877). After rinsing in TBS-T, grids were incubated with 20-nm gold-conjugated anti-rabbit secondary antibody (1:20, ab27237), for 1h at room temperature, rinsed in TBS-T and double-distilled water, air-dried, and examined with a Philips CM12 transmission electron microscope (Philips/FEI, Eindhoven, The Netherlands). The specificity of the immune reactions was tested by omitting the primary antibody.

3.6 Morphometric Analyses

For each experimental group (N = 8), we used a digital camera SIS MegaView III (Olympus Soft Imaging Solutions, Münster, Germany) to capture electron micrographs of 19 randomly selected white adipocytes at 17,000× magnification. We selected all white adipocytes to include both the nuclear and cytoplasmic areas, from all adipose tissue depots. To overcome variations in white adipocyte size when quantifying peroxisomes, DAB-positive organelles were counted per cell area (μm^2), and subsequently normalized to a 100 μm^2 area.

3.7 Fractal Analysis

All images for quantitative analysis were saved in the lossless TIFF format. For each tissue, a minimum of 20 electron micrographs were analysed per experimental group, with approximately five to seven images per animal. Fractal dimension and lacunarity were determined from catalase immunohistochemically-stained micrographs. Images were captured using a 100x objective lens on a Leica DMLB light microscope at a resolution of 2592x1944 pixels. These parameters were quantified on binarised and outlined images using the box-counting method, a well-established approach for assessing tissue complexity and heterogeneity using the FracLac plug-in (Karperien A. FracLac for ImageJ. Published 2013. Accessed [October 29, 2025]. https://imagej.net/ij/plugins/fraclac/FLHelp/Introduction.htm) for ImageJ (NIH, Bethesda, MD, USA). To enable direct correlation between chromatin structural complexity and nuclear dimension, the nucleus diameter was measured on the exact same micrographs.

3.8 Statistics

All obtained data were analyzed by the software GraphPad Prism (GraphPad Prism, Version 8.4.3, San Diego, CA, USA). Normal distribution was tested by D'Agostino and Pearson's normality test. Analysis of variance with multiple comparisons (One-way ANOVA) with Dunnett's post hoc tests was used for evaluating the differences between groups

For the fractal analysis and lacunarity statistical analysis were performed using the non-parametric Kruskal-Wallis test to assess the overall differences between the groups. If significant differences were found, pairwise comparisons between groups were then performed using the Dunn test for multiple comparisons. All statistical analyzes were performed using GraphPad Prism software. Results are expressed either as mean ± SD or ± S.E.M. of obtained values, and significances were set at $p<0.05$.

4. RESULTS

4.1 LIVER

4.1.1 Histological analysis of rat liver in methimazole-induced hypothyroidism

For histological analysis of liver tissue, e.g., gross appearance of liver lobes, the direction of hepatocytes rows, lipid bodies, glycogen and collagen amount, paraffin sections stained with hematoxylin, AZAN trichrome or periodic acid Schiff (PAS) were used.

Hypothyroidism did not cause changes in the structure and number of liver lobes compared to the control. Also, the position and size of hepatocytes, the orientation of hepatocyte rows, and lipid content were not affected (Figure 8).

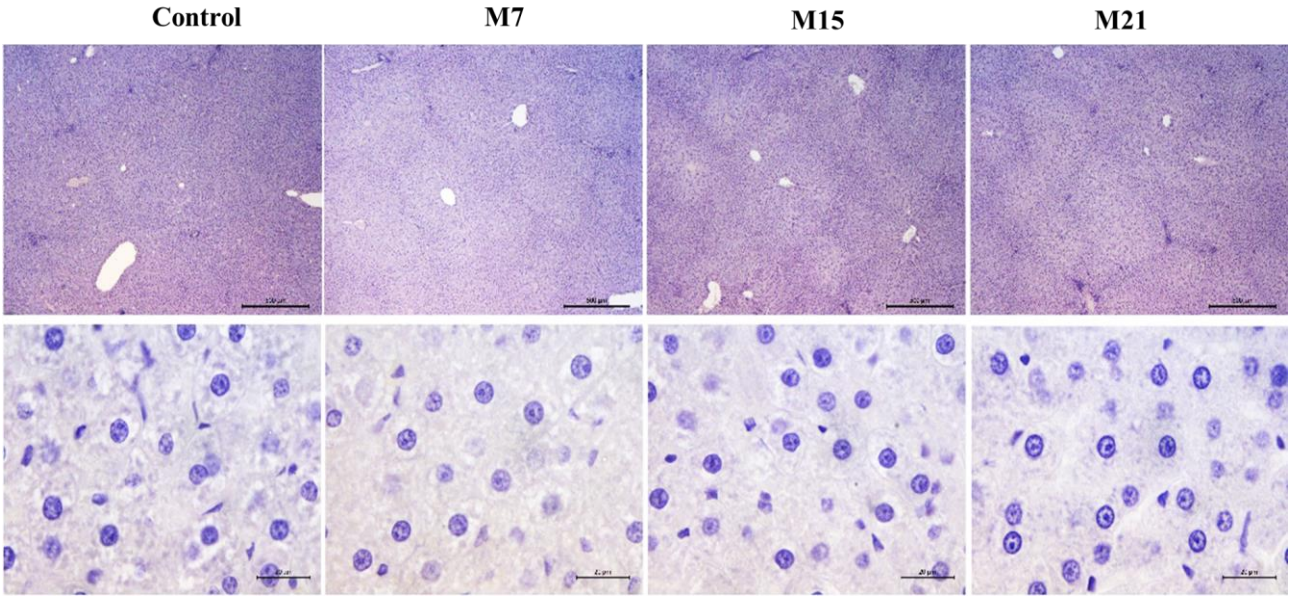

Figure 8. Hematoxylin-stained liver sections. Gross lobular anatomy and hepatocytes' appearance were not altered. Magnifications: upper row x10, orig.; lower row x100, orig. Scale bars: 500 μm (upper row) and 20 μm (lower row).

AZAN trichrome staining of liver sections showed nonsignificant but slightly lower prevalence of collagen in the extracellular matrix (ECM) in the M21 hypothyroid group (Figure 9). The volume density of the ECM in the control, M7, and M15 groups was 3.95, 3.98, and 4.03 % respectively, while in the M21 group it was 3.21 % of the relative tissue volume.

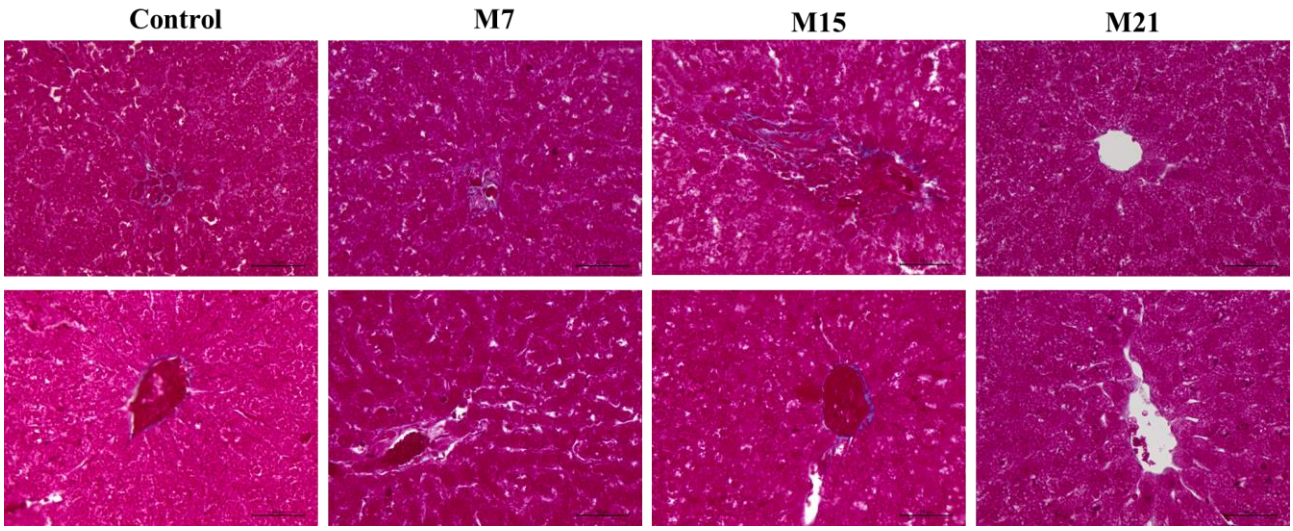

Figure 9. Normal distribution of collagen fibers within the portal areas and the sinusoids, together with the formation of connective tissue bridges between the portal areas (upper row). No signs/evidence of centrolobular fibrosis was observed (lower row). AZAN trichrome stain; x40, orig., scale bar 50 µm.

Glycogen presence in hepatocytes and its specific zonal distribution remained unaltered by hypothyroidism (Figure 10).

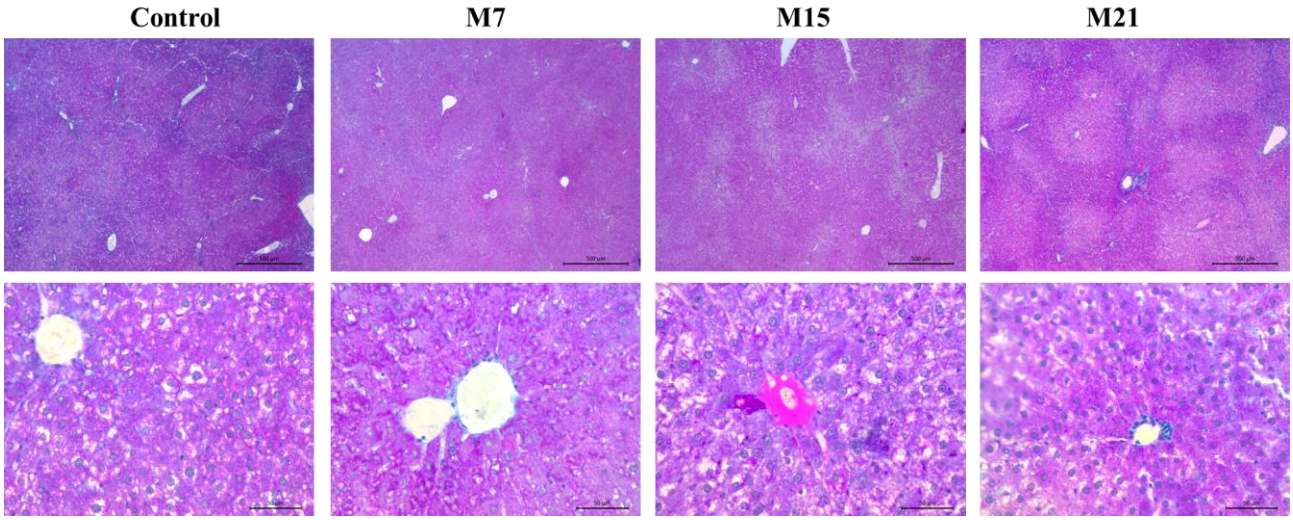

Figure 10. Histochemical staining for glycogen detection in rat liver by periodic acid Schiff (PAS). Magnification: x10, orig., bar 500 µm (upper row); x40, orig., scale bar 50 µm (lower row).

4.1.2 Ultrastructural analysis of rat liver in methimazole-induced hypothyroidism

Hepatocytes maintain lipid bodies, glycogen, and mitochondrial content while inducing peroxisomal biogenesis. Hypothyroidism alters hepatocytes' organellar association, leading to adaptive structural shifts in liver tissue. The association of organelles in hepatocytes typical for the control group is retained in groups M7 and M15 (Figure 11). Mitochondria associate with lipid bodies, the rough endoplasmic reticulum, peroxisomes, and glycogen depositions. The continuity of the gER and nuclear envelope is also present (Figure 12).

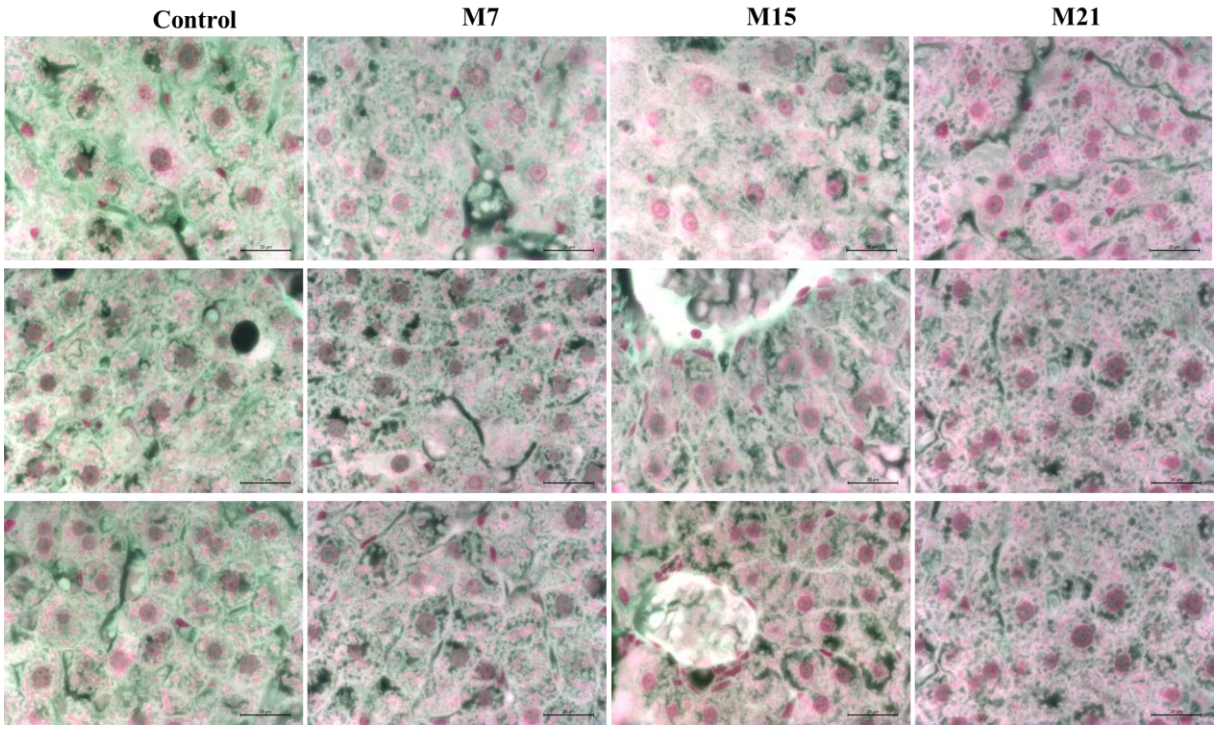

Figure 11. Organellar remodelling in hepatocytes. Paraffin liver sections stained for PAS, epifluorescence. Nuclei (pink); mitochondria (bright green); endoplasmic reticulum (dark green); lipid bodies (black); glycogen (light pink). Magnification: x100, orig., scale bar 20 μm.

Additionally, in M15 group where extensive peroxisomal biogenesis proceeds, very long and branched mitochondria were in close contact with transition of smooth and rough ER. In M7 and M15 groups, where binuclear cells were highly represented, two nuclei are connected with extensive transition of nuclear envelope and endoplasmic reticulum. Also, in the M21 group, the association of mitochondria with numerous peroxisomes was frequent.

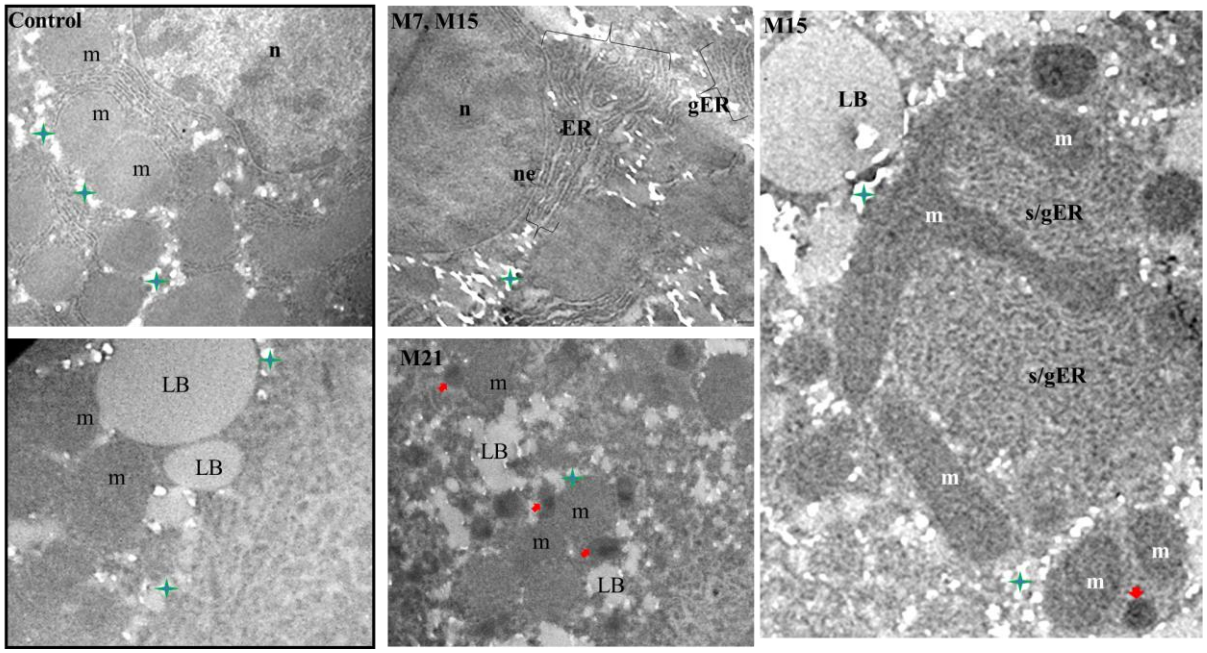

Figure 12. Organellar associations in hepatocytes. LB-lipid body; n-nucleus, ne-nuclear envelope; m-mitochondria; gER-rough (granular) endoplasmic reticulum; s/gER-smooth/rough (granular) endoplasmic reticulum. Glycogen (green star); peroxisome (red arrow). Magnification: x10000, orig.

4.1.3 Presence and distribution of hepatocytes with two nuclei (binuclearity)

Mononuclear hepatocytes constitute the majority of hepatocytes in the liver, especially in zone 1 and zone 3, whereas binucleated hepatocytes were more frequently observed in zone 2. Hypothyroidism decreases hepatocyte binuclearity exclusively in zone 2, and this was evident only in the M15 group (Figure 13).

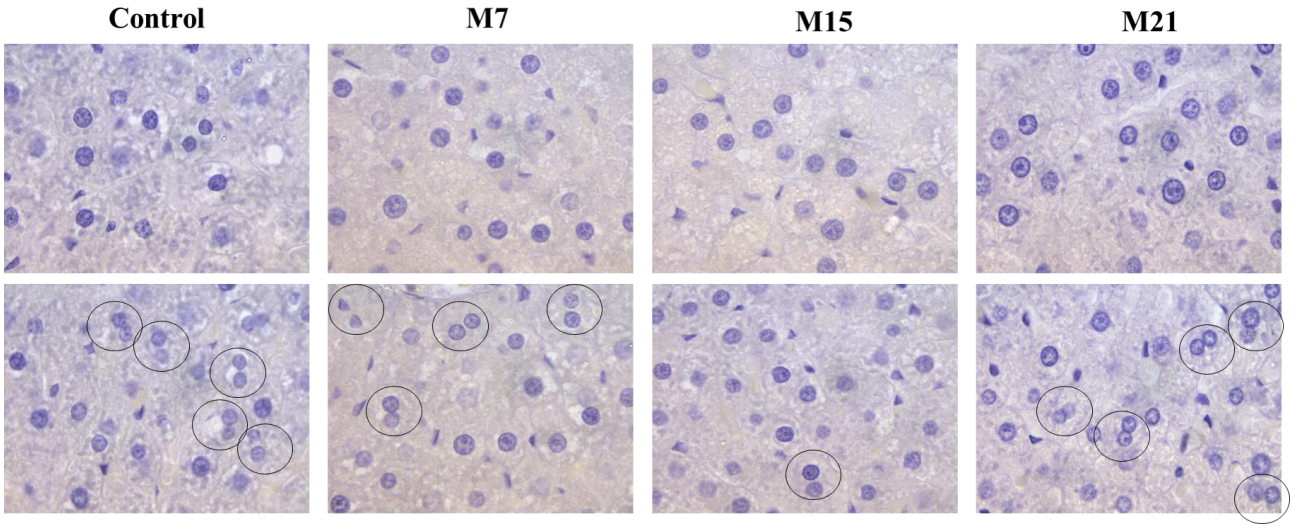

Figure 13. Mononuclear hepatocytes in the liver zone 1 and 3 (upper row), and binuclear hepatocytes in liver zone 2 (lower row). Hematoxylin staining. Magnification: x40, orig.

Additionally, AZAN trichrome-stained tissue sections revealed numerous dark-stained nuclei (a sign of mitotic competence) in control, M7 and M21, but not in M15 group (Figure 14A, 14B). Electron microscopic analysis revealed that those nuclei have chromosomes attached to deep invagination of nuclear envelope (Figure 14C).

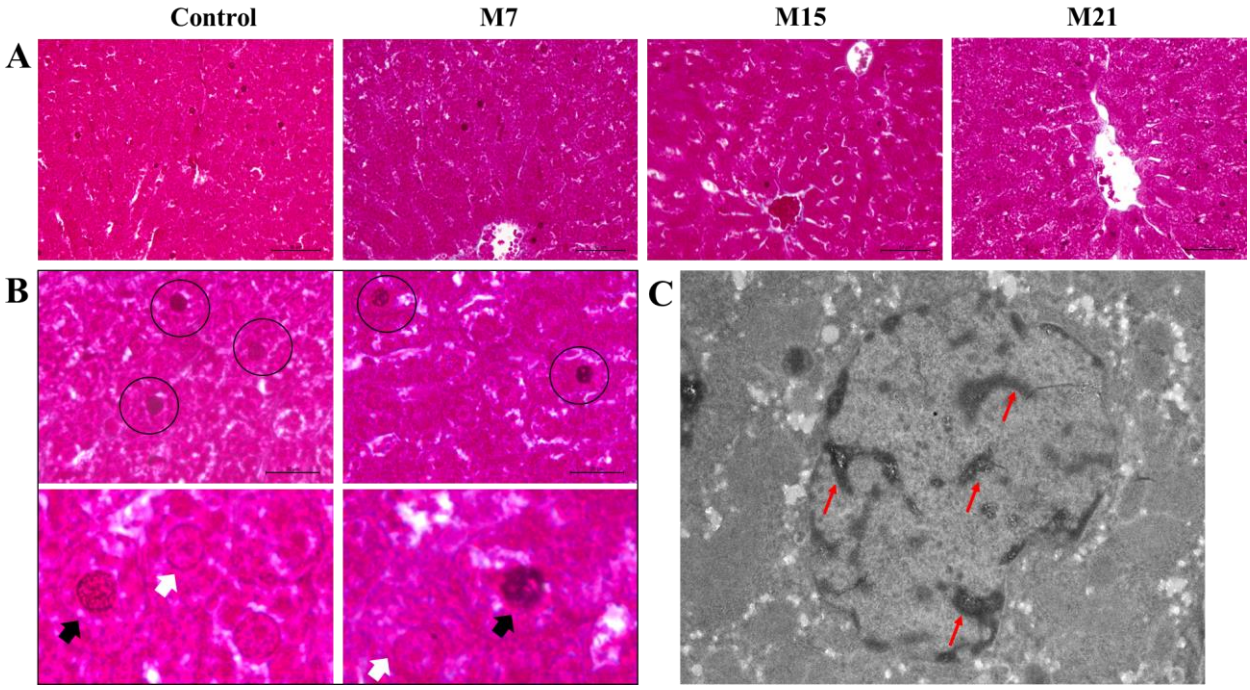

Figure 14. Presence of dark-stained nuclei in hepatocytes as a sign of mitotic competence (B circle and arrow). Ultrastructure of dark-stained nuclei shows chromosomes attached to deep nuclear invaginations (C, red arrow). AZAN trichrome staining (A, B); electron microscopy (C). Magnification: A-x40, org., scale bar 50 μm; B-x100, orig.; C- x6300.

4.1.4 Hypothyroidism induces appearance of nuclear condensates in rats' hepatocytes

Hypothyroidism induced the appearance of two types of nuclear condensates (condensates of biomolecules involved in the regulation of gene expression, RNA processing, and cellular stress responses) -fibrillar and granular (Figure 15). Fibrillar nuclear condensates were electron-dense and without a surrounding membrane. They were similar to nucleolar fibrillar centers and were predominantly observed in the vicinity of nucleolus. In contrast, granular nuclear condensates were localized at the periphery of nucleus, nearby nuclear pores. These condensates were absent in euthyroid control hepatocytes.

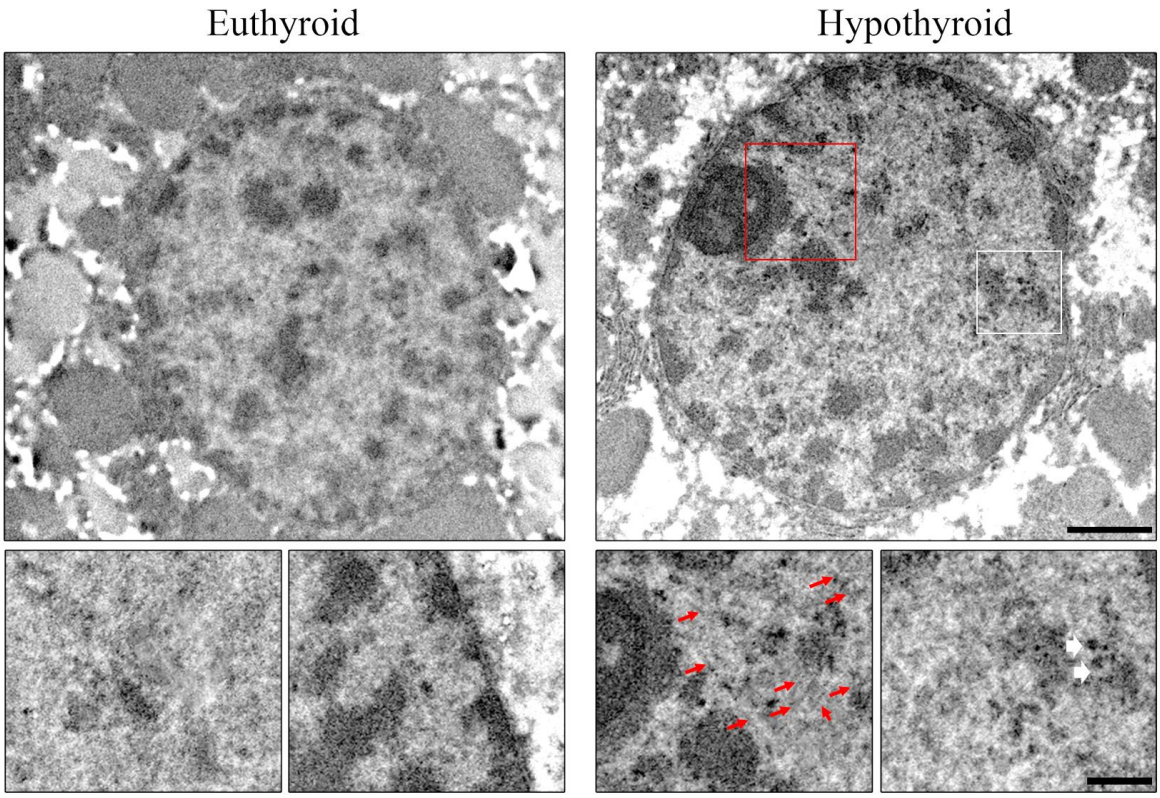

Figure 15. Ultrastructure of hepatocytes nuclei from euthyroid and hypothyroid rats. Fibrillar nuclear condensate (red rectangle and arrows); granular nuclear condensate (white rectangle and arrows). Scale bars: upper row 1 μm, and lower row 500 nm.

4.1.5 Hypothyroidism induces peroxisome biogenesis

Catalase immunofluorescent detection revealed a gradual increase in peroxisome abundance in hepatocytes over time-course of hypothyroidism (Figure 16). Pericentral hepatocytes displayed higher peroxisome density, whereas a distinct zonal gradient extending through zones 2 and 3 was observed, particularly in the M15 group. The unusual extraperoxisomal localisation of catalase was found in hepatocyte nuclei in both, M7 and M15 groups.

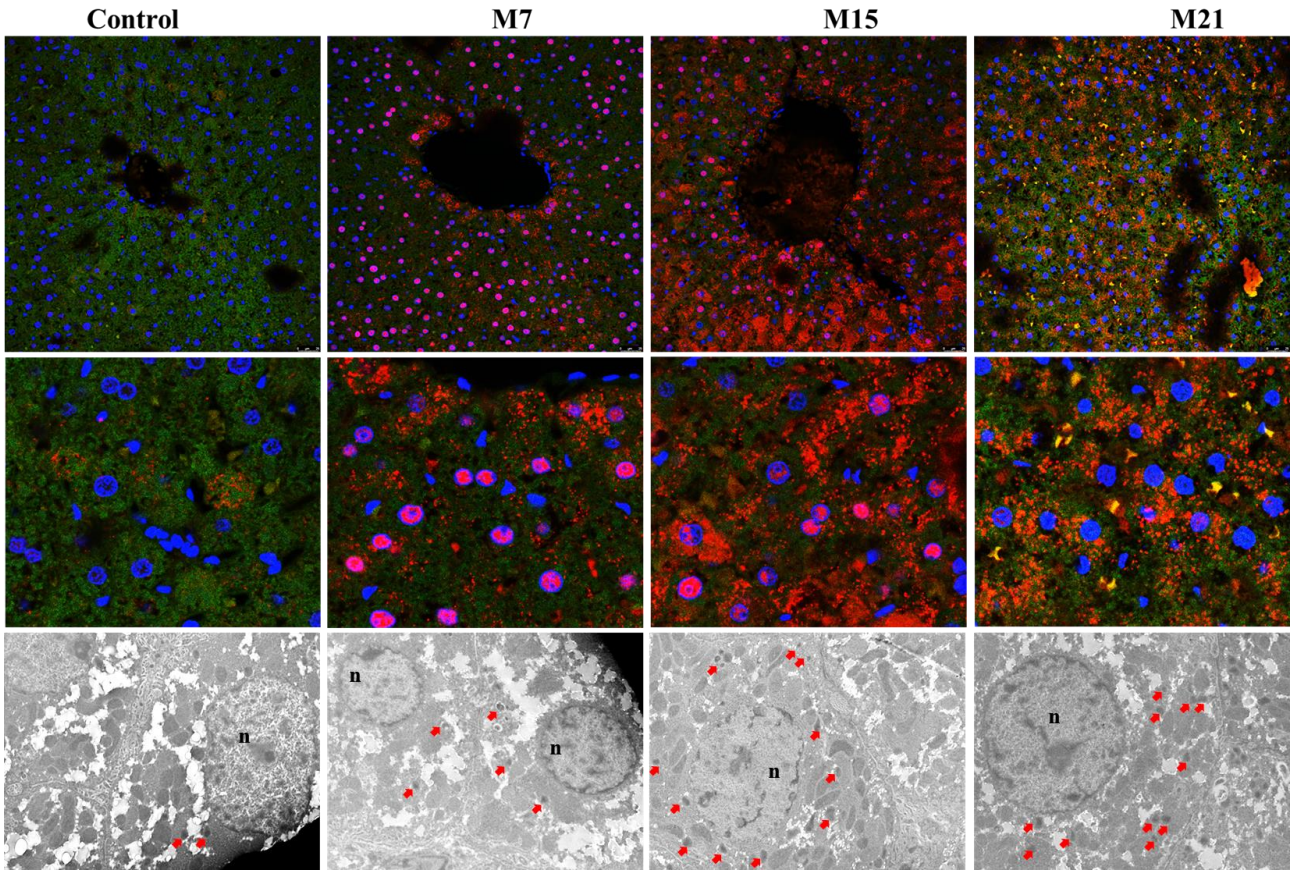

Figure 16. Hypothyroidism induces peroxisome biogenesis in hepatocytes. Catalase immunofluorescent detection (upper and middle rows, red signal) and ultrastructural appearance of peroxisome (lower row, red arrow). Peroxisomes show a clear gradient, which is highest in hepatocytes surrounding the central veins, especially in M15 group. Note nuclear positivity for catalase in M7 and M15 groups (pink signal). Magnification: x10-upper row; x40-middle row; x6300, orig. -lower row.

4.1.6 Hypothyroidism increases nuclear catalase immunopositivity in hepatocytes

Immunofluorescent labeling of catalase revealed its presence within hepatocyte nuclei. In order to reveal exact position and ratio of catalase-positive and catalase-negative nuclei, a routine immunohistochemical staining was applied (Figure 17). In control, catalase-positive nuclei were present in the pericentral and midlobular parts of the liver. Hypothyroidism induces higher catalase positivity of hepatocyte's nuclei in all three metabolic zone of the liver. In M7 and M15 groups, nuclear positivity was very high, while in M21 it was lower in periportal and pericentral parts comparing to control. Also, hepatocytes show substantial heterogeneity regarding simultaneous presence of catalase in nuclear and cytoplasmic (peroxisome) compartments. While some cells display only nuclear catalase positivity, others possess catalase positivity in both compartments.

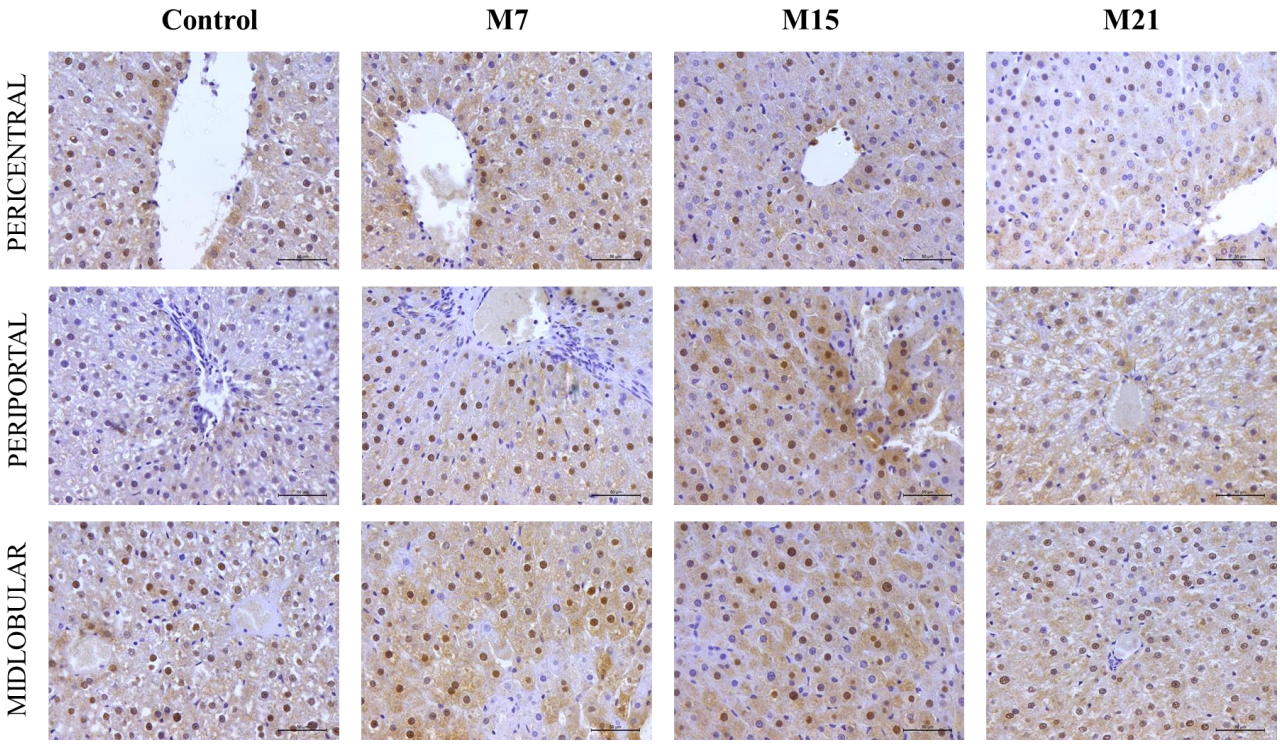

Figure 17. Catalase immunohistochemical detection in pericentral, periportal and midlobular part of rat liver. Magnification: x40 orig., scale bar 50 μm.

4.1.7 Hypothyroidism causes changes in chromatin state of hepatocyte nuclei

To investigate the potential relation of chromatin state changes with catalase immunopositivity in hepatocyte nuclei, fractal dimension and lacunarity to assess open vs. closed state of chromatin were analysed.

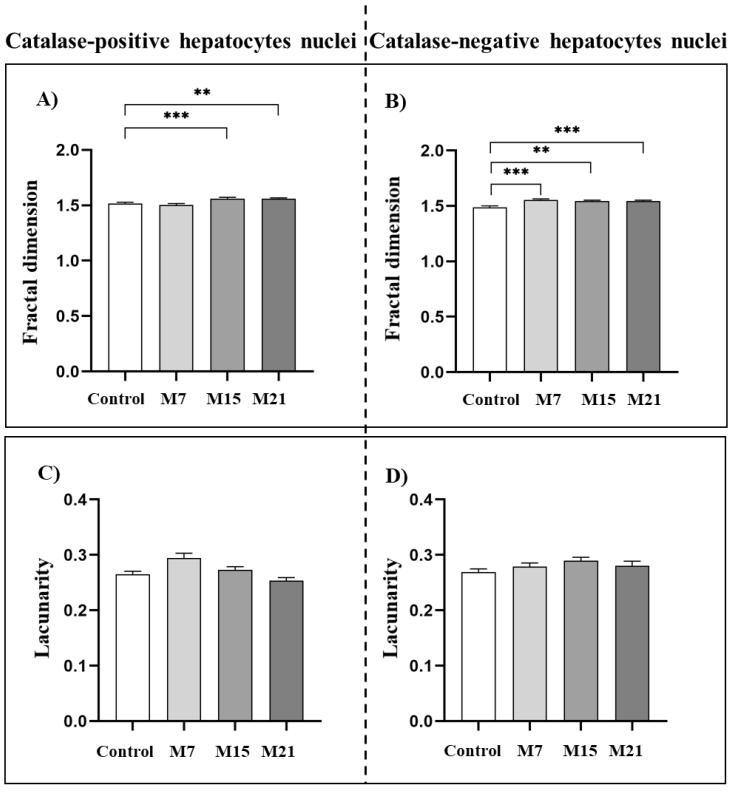

Figure 18. Fractal dimension and lacunarity in hepatocyte nuclei in hypothyroidism. *Compared to control, **p < 0.01, ***p < 0.001.

Fractal analysis revealed changes in fractal dimensions in the catalase-positive and catalase-negative hepatocyte nuclei of methimazole-treated, hypothyroid rats. Although the pattern of the changes was similar, an increase in fractal dimensions was more rapid in catalase-negative nuclei (observed in M7 group) compared with catalase-positive nuclei (detected in M15 group), as presented (Figure 18A, 18B). Also, once established, the change remained at the same value over the course of hypothyroidism. Unexpectedly, the lacunarity was stable over the course of hypothyroidism, irrespective of the catalase-positivity in hepatocyte nuclei (Figure 18C, 18D).

4.1.8 Average nuclear diameter distribution

Considering observed differences in fractal dimensions and stable lacunarity values in hepatocytes nuclei, irrespective of catalase immunostaining, the nuclear diameter of hepatocytes was measured (Figure 19). The results revealed a clear trend in the distribution of the average nuclear diameter with the treatment duration. Compared to the control group, where most nuclei diameters cluster around 11 µm, a clear shift towards smaller nuclei (around 7 µm) was observed with increasing treatment duration. This reduction in nuclear diameter indicates treatment-dependent alterations in hepatocyte nuclear morphology, consistent with adaptive cellular remodeling induced by hypothyroidism.

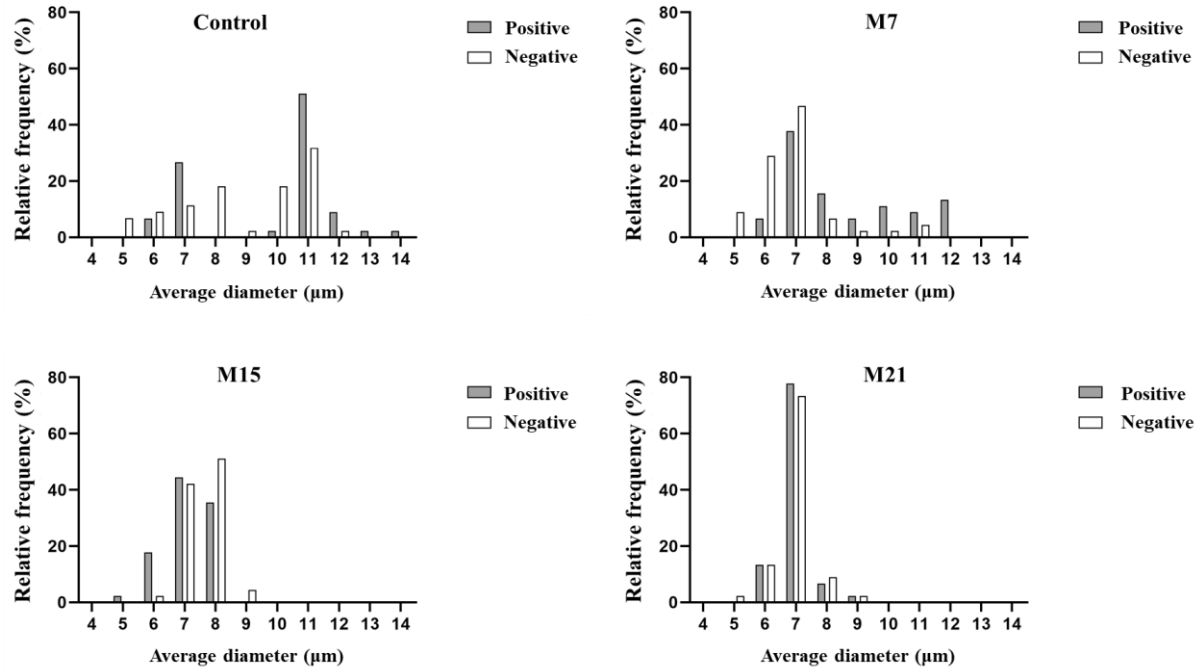

Figure 19. Average diameter of hepatocytes nuclei (µm) positive (gray) or negative (white) for catalase immunoexpression.

4.1.9 Antioxidant defense in rat liver in methimazole-induced hypothyroidism

Methimazole treatment did not induce changes in the activity of MnSOD (B) and CuZnSOD (C) at any examined time point (Figure 20). However, total GSH content was decreased in M15 and M2 groups in comparison to control (Figure 21A). Also, the activities of GSH-Px (Figure 21B), GR (Figure 21C), and GST (Figure 21E) were decreased after prolonged methimazole treatment (in M15 and M21 groups, respectively), while catalase activity was not affected by the treatment at any time point (Figure 21D). Contrary to the GSH-dependent part of antioxidant defense, the activity of TR was increased compared to control in M7 and M15 groups (Figure 21F).

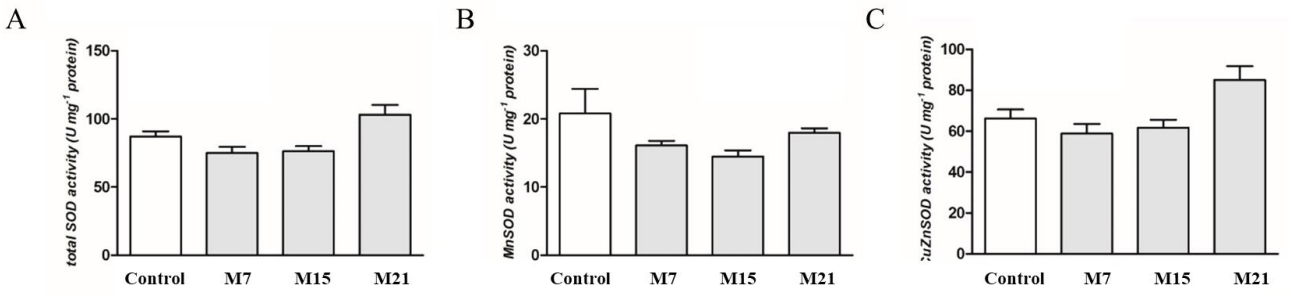

Figure 20. The activity of total superoxide dismutase (total SOD, A), manganese SOD (MnSOD, B) and cooper-zinc SOD (CuZnSOD, C) in the liver of control and methimazole-treated groups. Bars represent the mean ± S.E.M of six animals per group.

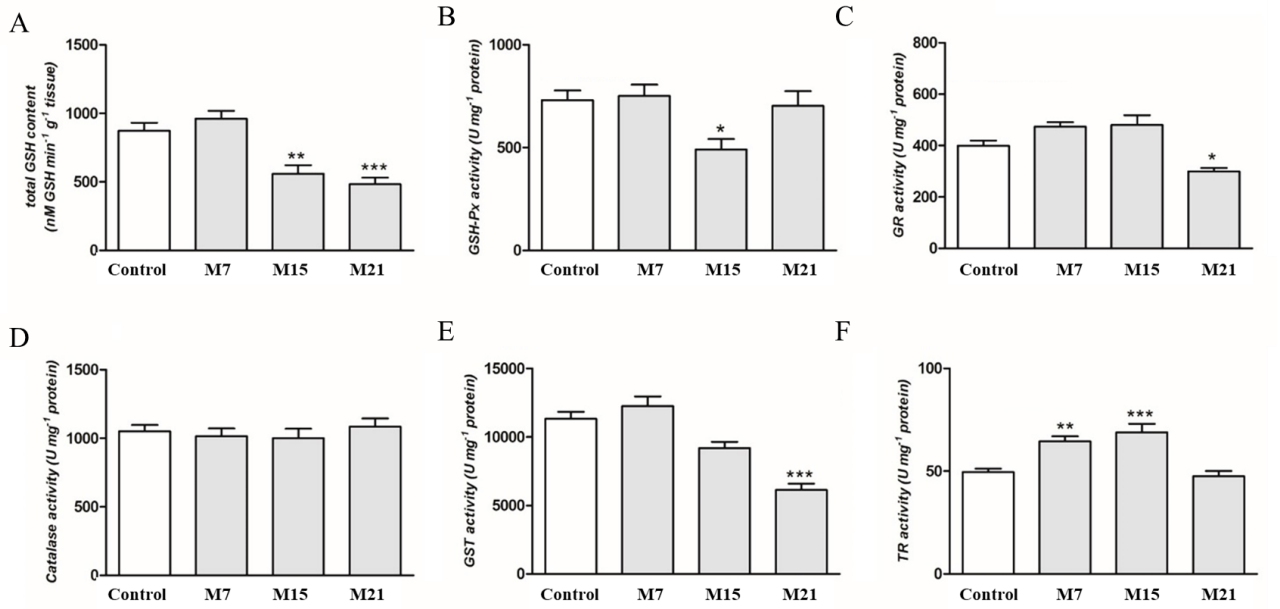

Figure 21. Changes in total glutathione (GSH, A) and activities of glutathione peroxidase (GSH-Px, B), glutathione reductase (GR, C), catalase (D), glutathione S-transferase (GST, E), thioredoxin reductase (TR, F) in methimazole-treated groups. Bars represent the mean ± S.E.M of six animals per group. *Compared to control, *$p < 0.05$, **$p < 0.01$, ***$p < 0.001$.

4.2 WHITE ADIPOSE TISSUE

4.2.1 Histological analysis of rat white adipose tissue in methimazole-induced hypothyroidism

For histological analysis of adipose tissue, e.g. gross appearance of adipocytes, the presence of macrophages, mast cells and connective tissue, resin-embedded tissue sections stained with toluidine blue were used.

Hypothyroidism did not cause gross changes in the structure and number of adipocytes compared to the control. Also, the presence of macrophages, mast cells and fibrosis was not noticed. However, heterogeneity among white adipocytes regarding size was clearly visible (Figure 22).

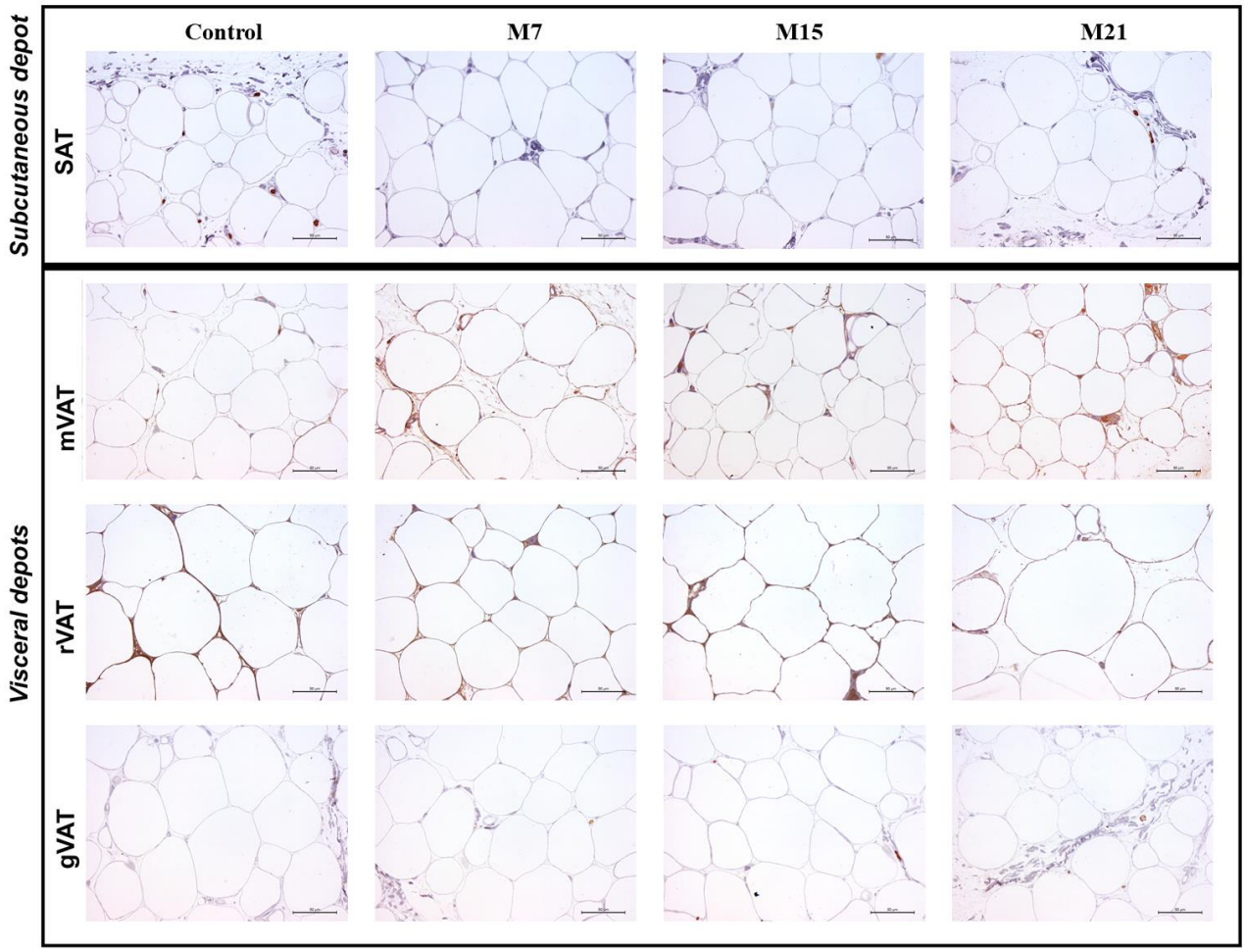

Figure 22. Toluidine blue-stained SAT depot and VAT depots semi-fine tissue sections. Gross anatomy and white adipocyte appearance were not altered. Magnifications: x40, scale bar: 50 μm.

4.2.2 Hypothyroidism induces peroxisome biogenesis in both SAT and VAT in a depot-specific manner

Peroxisomes labeled with DAB were used to investigate peroxisomal abundance in white AT depots in hypothyroidism. Peroxisome quantification demonstrated an increase in peroxisomal number over time in all analyzed white AT depots, yet with evident differences (Figure 23, Table 3).

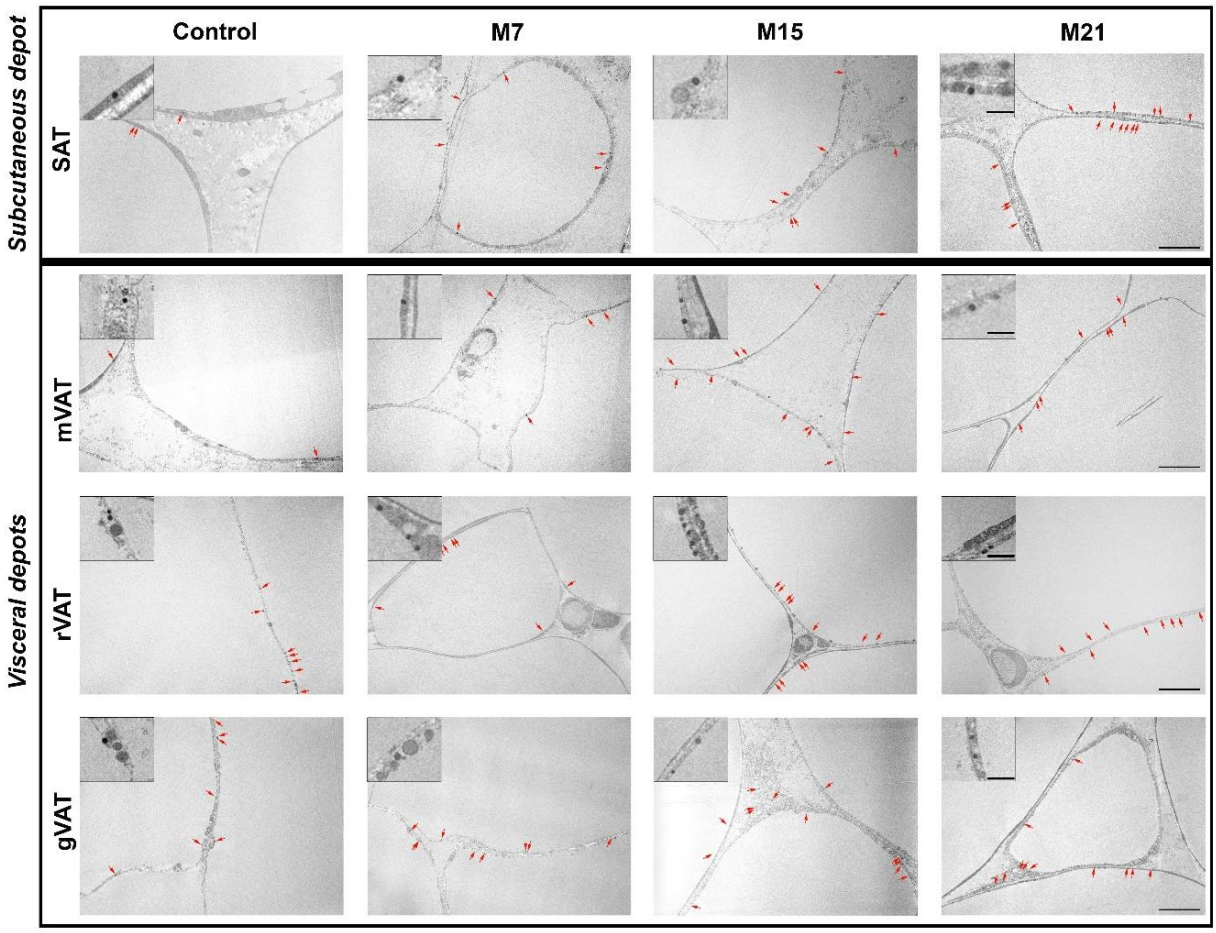

Figure 23. Representative electron micrographs of DAB-labeled peroxisomes (arrow) in SAT and VAT depots of white AT from control and hypothyroid rats treated with methimazole for 7, 15, or 21 days. Insets: magnified area with DAB-positive peroxisome. Scale bar: 2 µm and insets:250 nm.

rVAT and gVAT of euthyroid controls showed a higher number of peroxisomes compared to mVAT and SAT controls (Figure 23). Hypothyroidism rapidly induced an increase in peroxisome number in all SAT and VAT depots (M7 group). In gVAT, the number of peroxisomes continued to rise steadily throughout the 21-day treatment (M21 group), whereas in mVAT, rVAT and SAT, the changes were unequal.

Table 3. The average peroxisome number per 100 μm^2 area of white adipocytes.

Average peroxisome number/100 μm^2 area of white adipocytes				
Depot	**Control**	**M7**	**M15**	**M21**
SAT	3.188±0.274	5.395±0.674***	4.853±0.468***	6.836±0.721***
mVAT	2.404±0.612	6.891±0.780***	6.535±0.804***	8.242±1.020***
rVAT	3.891±0.590	5.943±0.831***	5.717±0.784***	6.233±0.771***
gVAT	4.812±0.592	6.464±0.932***	9.821±1.437***	10.894±1.652***

Mean values ± SD are represented. *Compared to the control value. ***, $p < 0.001$.

In all of examined depots (SAT and VAT), peroxisome biogenesis predominantly proceeded via the canonical pathway, characterized by growth and division of existing elongated peroxisomes (Figure 23). In rVAT and gVAT, hypothyroidism also activated the *de novo* pathway, characterized by peroxisomal budding from endoplasmic reticulum, although in a different manner. In gVAT, the

de novo pathway was observed only in M7 group, while rVAT showed a more complex pattern. In rVAT, the *de novo* pathway was already functional in euthyroid control, and it was further enhanced by hypothyroidism, causing a time-dependent increase in peroxisomal number with the peak in M15 group (Figure 24).

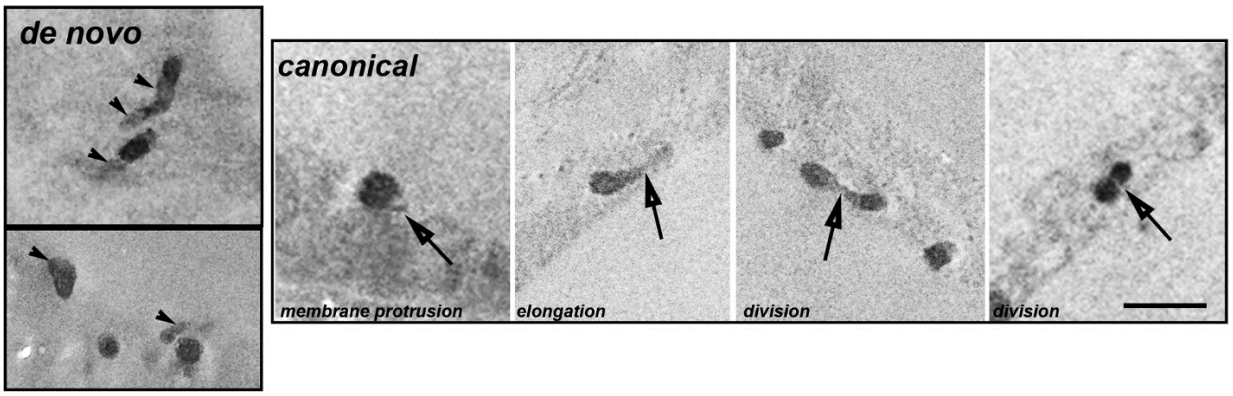

Figure 24. Peroxisome biogenesis in white adipocytes by *de novo* pathway and by the canonical pathway through growth and division. Representative electron micrograph with DAB-labeled peroxisomes in white adipocytes cytoplasm of VAT depots. *De novo* pathway (in gVAT in M7 group and in rVAT in M15 group) is characterized by several interconnected peroxisomes (arrowhead) originating from endoplasmic reticulum. Canonical pathway present in all examined SAT and VAT depots begins with the formation of a membrane protrusion followed by peroxisomal elongation and division (arrow). Scale bar: 250 nm.

Peroxisomes were located close to lipid bodies independently of either treatment or examined depots (SAT and VAT) (Figure 25). They were often attached to mitochondria (Figure 25). Prominent presence of the endoplasmic reticulum was expectedly observed only in rVAT and in gVAT in M7 group as a consequence of *de novo* peroxisomal biogenesis (Figure 25, rVAT, gVAT).

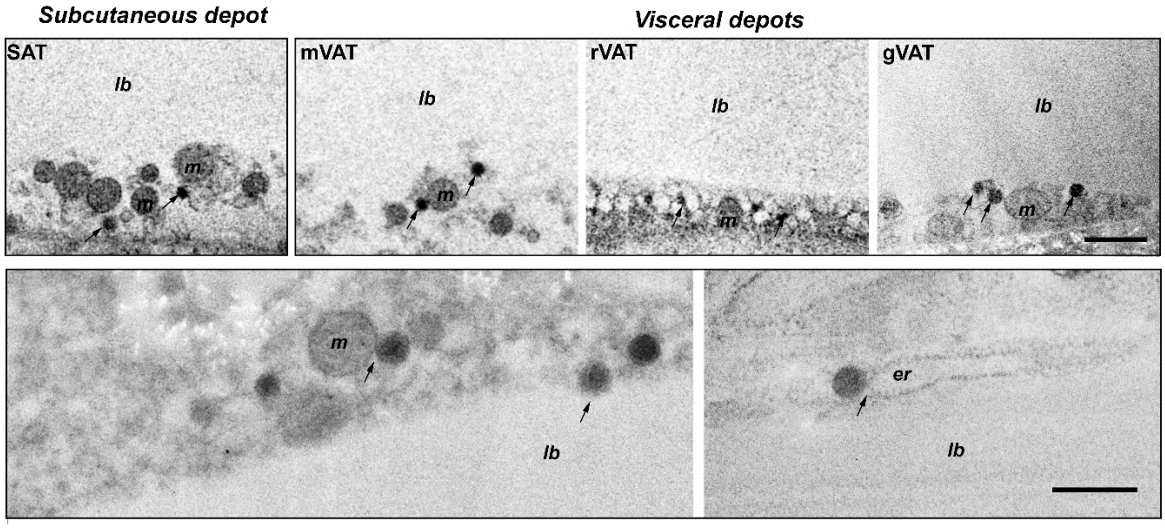

Figure 25. The localisation of peroxisomes in white adipocytes after 7 days of methimazole treatment (first row). Peroxisomes (first row, arrow) are predominantly located adjacent to the lipid body (lb) or in their vicinity. Additionally, they are often attached to mitochondria (m). Magnified representative area (second row) shows contact (arrow) between peroxisome and mitochondria (m), lipid body (lb), or endoplasmic reticulum (er), respectively. Scale bar: first row-1μm; second row-500 nm.

4.2.3 Hypothyroidism changes the expression of peroxins Pex11β and Pex19 in white AT depots

Overall, hypothyroidism increased protein expression of both Pex11β and Pex19 in all examined AT depots, with variations observed over time. In SAT, mVAT and gVAT, an increase in Pex11β level was evident immediately in M7 group, while in rVAT, it was delayed (Figure 26). On the contrary, an increase in Pex19 expression took longer in all depots except mVAT (M7 group).

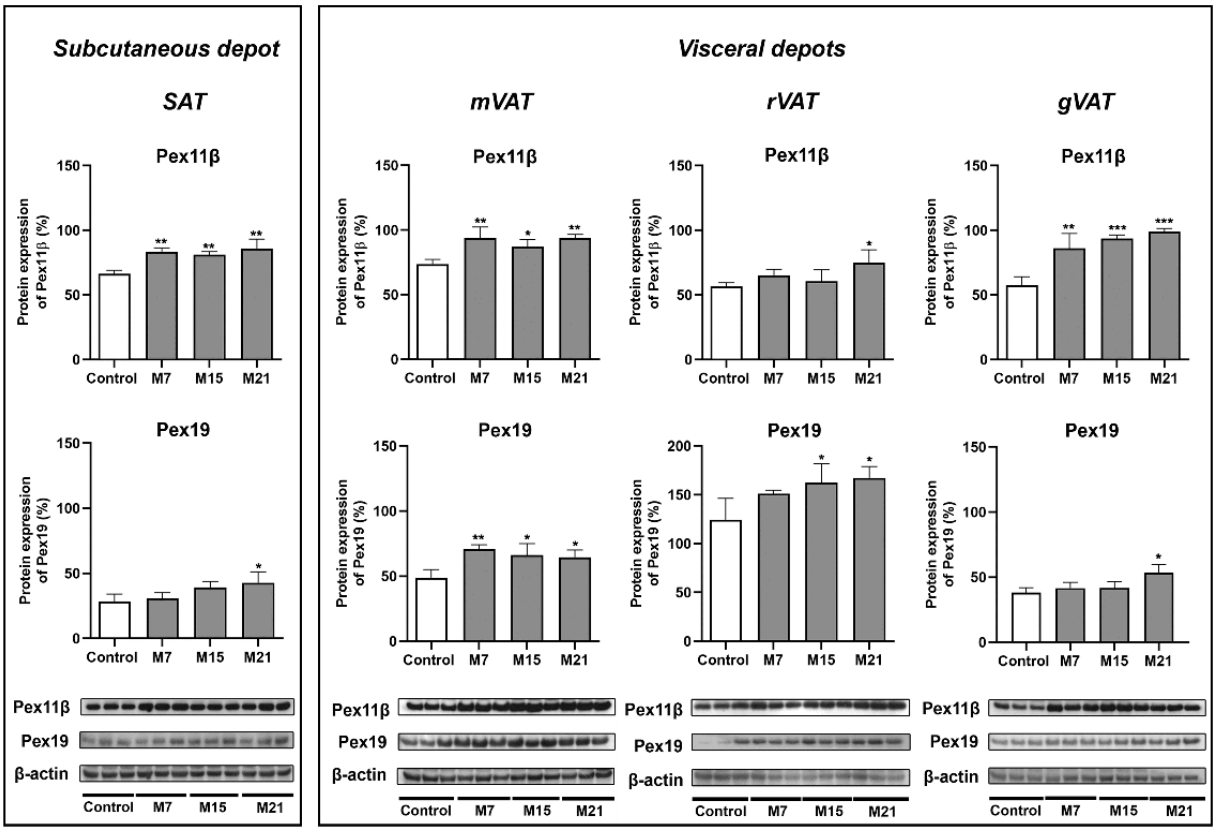

Figure 26. Protein expression of Pex11β and Pex19 in SAT and VAT depots of white AT from control (white) and hypothyroid (grey) groups treated with methimazole for 7, 15, or 21 days. Data shown represent the average values of target protein bands normalized against those of beta-actin, along with their representative blots (N=3 per group);*Compared to control group, $*p < 0.05$, $**p < 0.01$, $***p < 0.001$.

4.2.4 Hypothyroidism changes PPARα protein expression differently in SAT and VAT depots

PPARα basal expression was significantly higher in SAT and mVAT than in other VAT depots, and hypothyroidism did not cause any change in its expression (Figure 27). However, there was a significant increase in PPARα levels in rVAT and gVAT during hypothyroidism. In gVAT, this increase was transient, occurring only in M7 group.

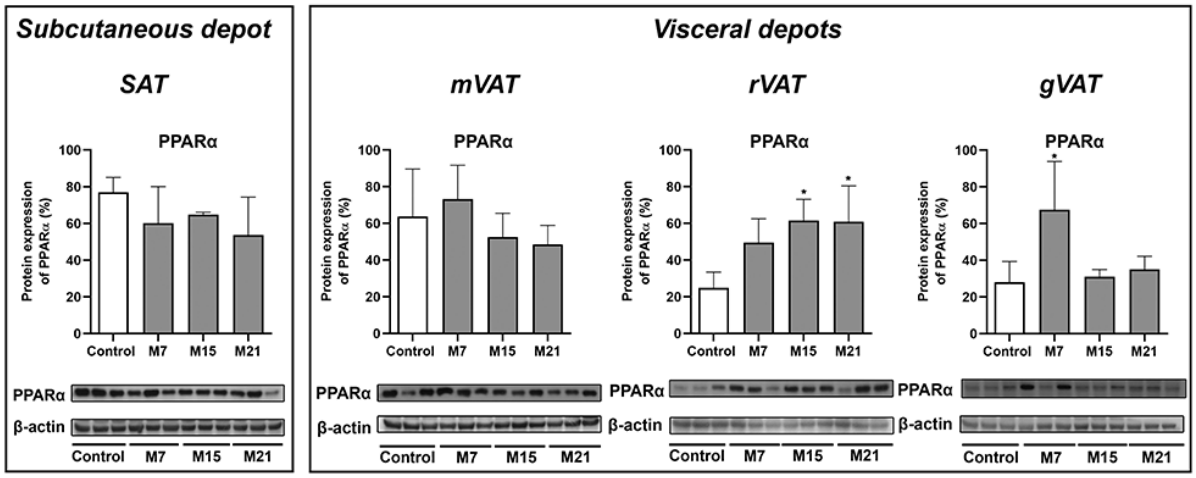

Figure 27. Protein expression of PPARα in SAT and VAT depots of AT from control (white) and hypothyroid (grey) groups treated with methimazole for 7, 15, or 21 days. Data shown represent the average values of target protein bands normalized against those of beta-actin, along with their representative blots (N=3 per group);*Compared to control group, ∗p < 0.05.

4.2.5 Hypothyroidism causes the appearance of a pexopodium-like structure in VAT but not in SAT

Numerous structures resembling peroxisomal protrusions – pexopodium were observed in all VAT depots, but not in a SAT (Figure 28). These pexopodium-like structures were visible toward the lipid body's interior in adipocytes with noticeable differences between different depots of VAT. The pexopodium-like structures (arrowhead) appeared only in visceral depots, in mVAT and rVAT from day 15 of hypothyroidism, and on day 21 in gVAT. They were DAB positive, larger than peroxisomes, and had a semi-spherical form (Figure 28).

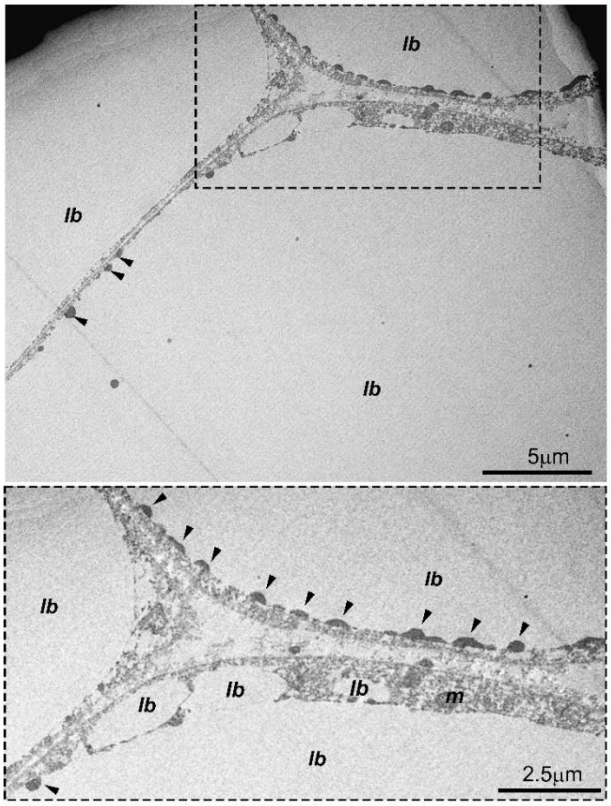

Figure 28. Presence of unusual pexopodium-like structures (arrow) that invaded lipid body's (lb) interior from their very surface was observed in white adipocytes. Pexopodium-like structures appeared in all VAT depots but not in the SAT depot. Representative electron micrographs from rVAT. Box represents magnified area. m-mitochondria. Scale bar: 2.5 μm and 5 μm.

Based on the proposed role of pexopodia and their localization within lipid bodies, as well as their association with peroxisomes observed in the present study, immunogold labelling of ACOX1 was performed. The analysis was conducted in the VAT depot and at the time point exhibiting the highest abundance of pexopodium-like structures (rVAT, M15). ACOX1 immunoreactivity was detected exclusively in peroxisomes (arrows), whereas pexopodium-like structures were devoid of ACOX1 labelling (arrowheads) (Figure 29A-D). Nevertheless, some ACOX1-positive peroxisomes were found in close association with pexopodium-like structures (Figure 29D, circle).

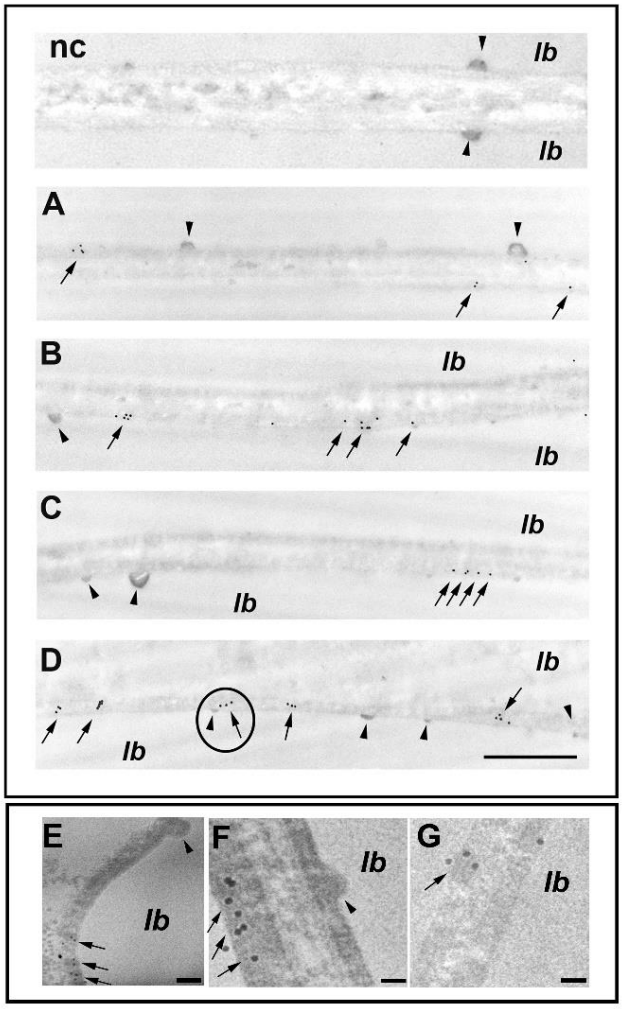

Figure 29. Immunogold labeling of ACOX1 in the rVAT adipocytes (A-G) in M15 group. Peroxisomes (arrow) are loaded with ACOX1, while pexopodium-like structures (arrowhead) remained unlabeled. In some cases, an ACOX1-labeled peroxisome is observed in close association with pexopodium-like structures (D, circle, arrowhead). nc – negative control; lb – lipid body. Scale bar: (A-D) 1 µm; (E, G) 100 nm

Further, immunogold labelling of catalase was performed. Pexopodium-like structure in rVAT adipocytes of M15 group (group and depot with numerous pexopodium-like structures) was mostly catalase-negative (white arrow), although a small number were catalase-positive (red arrow). Furthermore, membranous areas positive for catalase on lipid bodies, near cytoplasm and also deep inside the lipid body interior, were observed (Figure 30).

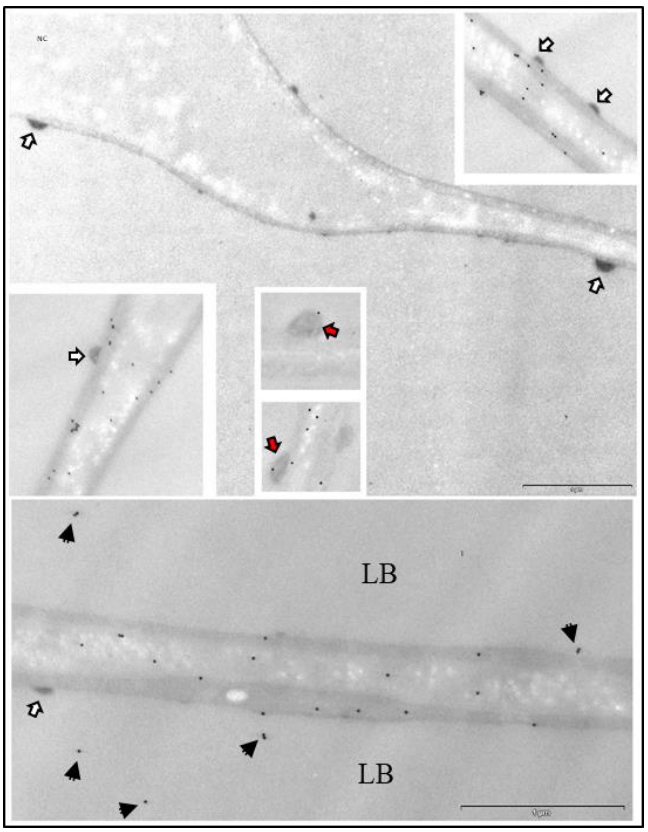

Figure 30. Immunogold labeling of catalase in adipocyte from retroperitoneal AT depot (rVAT). Pexopodium-like structures were mostly catalase-negative (white arrow), although a small number were catalase-positive (red arrow). Some membranous catalase-positive areas of lipid body (LB) were on the side in contact with the cytoplasm but also deep inside in the LB interior. NC - negative control. Magnification: insets-x17000 org., scale bar 1µm.

5. DISSCUSION

5.1 Structural alteration of hepatocytes in methimazole-induced hypothyroidism

The high prevalence of hypothyroidism in patients with NAFLD and the involvement of thyroid dysfunction in the pathogenesis of NAFLD are documented (Vidal-Cevallos *et al.*, 2023; Pu *et al.*, 2025), but the association of low-normal thyroid function (LNTF) with NAFLD or metabolic dysfunction-associated fatty liver disease (MAFLD) is still controversial (Liu *et al.*, 2018; Zuarth-Vázquez *et al.*, 2023; Abeysekera *et al.*, 2020).

Methimazole-induced hypothyroidism did not cause pathological changes in the liver, but rather fine-tuned adaptations by the assembly of organelles in hepatocytes. This is the first data regarding structural adaptation of hepatocytes to lipid disturbance in hypothyroid conditions.Through peroxisomal biogenesis and increased catalase in the nuclei, hepatocytes were increased their resistance to lipotoxicity and protected DNA from oxidative damage.

5.2 Antioxidant defense alterations in rat liver in methimazole-induced hypothyroidism

Thyroid hormones play an important role in regulation of whole-body metabolism. However, the data of the effects of hypothyroidism, especially the effects of methimazole-induced hypothyroidism on intracellular redox and antioxidant status in the liver are not consistent. Herein we showed that methimazole-induced hypothyroidism drives reorganization in the antioxidant defense in the rat liver in time-dependent manner: while there were no changes in the activity of superoxide dismutases (CuZnSOD and MnSOD), the activity of GSH-dependent part of AD including GSH-Px, GR and GST, along with the total GSH level, was decreased in M15 group (total GSH, GSH-Px) and in M21group (GR and GST). In contrast, the activity of TR was increased in M7 and M15 groups comparing with control. These changes in antioxidant defense in the liver could reflect the effects of methimazole-induced hypothyroidism and/or methimazole itself on intracellular oxidant/antioxidant balance.

Bearing in mind the mode of action of thyroid hormones on tissue metabolism, the observed decrease in GSH-dependent part of antioxidant defense in M15 and M21 groups could be described as an adaptive response on suppression of metabolism due to prolonged methimazole treatment. Liver is continuously challenged with the high oxidative pressure as a result of the high metabolic activity, thus appropriate adaptive response of antioxidant defense is crucial for maintaining the tissue redox homeostasis in the cases of metabolic instabilities. However, the present literature data considering the effects of hypo- and hyperthyroidism on the production of ROS and antioxidant defense organization in many tissues are inconsistent, showing nonlinear ratio between respiration rate and ROS production. For example, hypothyroidism does not modify (Venditti *et al.*, 1997), reduce (da Rosa Araujo *et al.*, 2010) or even increase (Sahoo *et al.*, 2008; Gariani and Jornayvaz, 2021) oxidative damage in metabolically active organs. Guerrero *et al.* (1999) reported that hypothyroidism increases oxidative pressure in mouse liver, most likely the consequence of the effects of thyroid hormones on cellular metabolism. Production of ROS is rather complex and involve several aspects of THs action: a) regulation of mitochondrial respiratory state, synthesis of respiratory chain elements (Horrum *et al.*, 1985), mitochondrial proton leak (Harper and Brand, 1994) and mitochondrial biogenesis (Mutvei and Nelson, 1989) and b) the expression of enzymes involved in ROS production and removal, like NADPH oxidase and nitric oxide synthase (Fernández *et al.*, 1985).

Considering the complexity of TR/ROS interplay, we should be cautious about conclusion that the decrease in GSH-related part of AD (GSH, GSH-Px and GR) is just adaptive response to hypometabolic status in hypothyroidism; actually this could as well be the reason for increased oxidative pressure. A noticeable imbalance in the responses of H_2O_2 producing and removing systems, along with no changes in SOD activity, could increase peroxidative pressure. An increase in

TR activity, as a part of peroxide-removing system complementary to GSH-dependent one supports this notion.

Decrease of the GST activity in M21 group also suggesting that liver major detoxifying role in drug metabolism could be compromised after prolonged methimazole treatment. This is in accordance with the previously published data that methimazole itself may induces liver toxicity (Cano-Europa *et al.*, 2010). The reduction of antioxidant defense and its relation with increased cellular damage in the liver in methimazole-induced hypothyroidism has also been reported (Das and Chainy, 2001). The results of the present study elucidate the effects of methimazole-induced hypothyroidism on antioxidant defense in the liver. It seems likely that methimazole treatment in a dose used therapeutically to reduce metabolic activity in hyperthyroidism leads to reorganization of antioxidant defense in the liver. Namely, the discrepancy in the changes in peroxide producing (SODs) and removing (GSH, GSH-Px and GR) systems represents specific response as a consequence of the newly established redox homeostasis. This indicates that specifically tailored antioxidant supplementation should be involved to restore the redox environment to balance.

5.3 Structural and redox alteration of white adipocytes in methimazole-induced hypothyroidism

This research provides new insights into depot-specific and time-dependent peroxisomal dynamics in rats white AT depots in hypothyroidism. Methimazole treatment drives coordinated, but heterogeneous responses across white AT depots involving Pex11β/Pex19 and PPARα, which mediate an increase in peroxisome abundance over the course of hypothyroidism. Distinct, depot-specific peroxisomal origins and the emergence of specific peroxisomal structures known as pexopodia were revealed, but ACOX1 immunolocalization does not support their direct involvement in β-oxidation. These structures probably reflect altered/aberrant fatty acid metabolism, characteristic of hypothyroid conditions.

Peroxisome-specific DAB labeling discovered a significant increase in peroxisome numbers in adipocytes of all analyzed AT depots. Further ultrastructural analysis confirmed that peroxisomal biogenesis in both SAT and VAT depots occurs via two common pathways: the canonical, by growth and division, and the *de novo*, by budding from the smooth endoplasmic reticulum. The primary pathway in white AT depots is the canonical pathway. However, a clear depot- and time-dependent divergence was observed in the activation of these pathways.

Pex11β, the constitutively expressed isoform of the Pex11 family, regulates peroxisome proliferation and controls their morphology, size, and number (Li and Gould, 2002; Koch *et al.*, 2005; Koch *et al.*, 2010; Thoms and Erdmann, 2005; Delille *et al.*, 2009; Farré *et al.*, 2019). It is the major peroxin that drives the canonical pathway of peroxisome biogenesis (Schrader *et al.*, 1998), while Pex19 is a multifunctional protein essential for assembly of the peroxisomal membrane and import of peroxisomal membrane proteins (Jones *et al.*, 2024). In addition to its role in the canonical pathway, Pex19 has also been shown to play a role in *de novo* biogenesis. It is required for the budding of pre-peroxisomal vesicles from the endoplasmic reticulum (Agrawal and Subramani, 2019). Our investigation revealed a time-course increase in the expression of Pex11β and Pex19 in all white AT depots, pointing to the gradual peroxisomal biogenesis in white AT of hypothyroid rats. SAT and mVAT showed an early increase in Pex11β expression and predominantly relied on peroxisome division, whereas visceral depots, particularly rVAT and gVAT, exhibited delayed induction of Pex11β (in rVAT) and Pex19 (in gVAT), suggesting depot-specific temporal differences in the mechanisms regulating peroxisomal expansion.

In addition, *de novo* peroxisome biogenesis from the endoplasmic reticulum was ultrastructurally detected in both rVAT and gVAT, but at distinct, non-coincident time points of hypothyroidism, while in SAT and mVAT depots, *de novo* peroxisome biogenesis was not observed at all. These

findings provide strong evidence for depot-specific alterations in peroxisome biogenesis triggered by hypothyroidism in white AT. The differences among distinct VAT depots are more pronounced than those observed between SAT and VAT. The significance of depot-specific variations in white AT during hypothyroidism remains undetermined. Peroxisome *de novo* biogenesis often involves increased Pex19 expression, but this pattern is not universal across all white AT depots, as shown by comparing inguinal and gVAT depots. Namely, cold exposure increases Pex19 expression in the inguinal depot but not in the gVAT depot (Park *et al.*, 2019).

Peroxisomes closely interact with lipid bodies – dynamic, single phospholipid-monolayer organelles - to regulate cellular lipid homeostasis (Walther and Farese, 2012; Welte, 2015; Olzmann and Carvalho, 2019). Specifically, the peroxisome bilayer and the lipid body monolayer may undergo hemifusion at points of physical contact to promote fatty acid transfer between these compartments. Consistent with their functional coupling, we observed close peroxisome-lipid body contacts across all examined time points. Within this context, a major finding of this study is the identification of pexopodium-like structures – peroxisomal extensions bridging to lipid bodies – which are uniquely present in visceral white adipocytes. While pexopodium structures were observed in VAT at various time points in the hypothyroid state, these structures were not present in SAT. This indicates a depot-specific structural adaptation of peroxisome-lipid droplet interactions, restricted to VAT under hypothyroid conditions.

Close physical contact between peroxisomes and lipid bodies is well documented in mammalian, yeast, and plant cells (Blanchette, 1966; Schrader, 2001; Aleksic *et al.*, 2021; Binns *et al.*, 2006; Kunze *et al.*, 2006; Gao and Goodman, 2015). Detailed immunocytochemical and ultrastructural analyses have shown that, depending on the species and conditions, peroxisomes form DAB-positive, hemispherical membrane projections termed pexopodia (Binns *et al.*, 2006; Goldberg *et al.*, 2009), peroxules (Thazar-Poulot *et al.*, 2015; Scholz *et al.*, 2022) or gnarls (Binns *et al.*, 2006) that enter the lipid body core. However, despite these observations in other experimental systems, the emergence and functional role of such structures in adipose tissue remain poorly understood. The presumed role of these structures may be to increase the surface contact between peroxisomes and lipid bodies as shown in some studies (Carmichael, 2023), resulting in accelerated lipolysis and increased free fatty acid availability for oxidation (Binns *et al.*, 2006).

Accordingly, an increase in PPARα protein levels was observed after 15 and 21 days of hypothyroidism in rVAT, i.e. after 7 days in gVAT, supporting the presumed role of pexopodia formation in fatty acid transfer and/or oxidation (Goto *et al.*, 2011). As the increase in PPARα was detected exclusively in adipose depots and coincided temporally with the presence of pexopodia, both features may reflect a common response of these AT depots characterized by enhanced fatty acid turnover, transport, and/or oxidation. However, further characterization of pexopodia through ACOX1 expression indicates that pexopodia, together with the observed elevated PPARα expression, may instead reflect an aberrant fatty acid oxidative VAT phenotype in hypothyroidism. Thus, to further characterize pexopodium-like structures, ACOX1 immunocyto-localisation was examined at its maximum level of appearance in rVAT. Although ACOX1 was present in white adipocytes' peroxisomes, the pexopodium-like structures showed no immunogold-positivity. These results suggest that pexopodium-like structures are likely not involved in the β-oxidation of fatty acids, but potentially act as a depot for fatty acids and/or other lipid metabolites. Detailed profiling of enzymatic pathways involved in peroxisomal fatty acid α-oxidation and lipid synthesis should reveal the mechanisms and pathophysiological relevance of unusual peroxisomal structures in hypothyroid VAT.

6. CONCLUSIONS

In this doctoral dissertation, the structural and redox alterations of the liver and white adipose depots (SAT and VAT) in methimazole-induced hypothyroidism were investigated, and the following conclusions were drawn:

- In hypothyroidism hepatocytes preserve their structure but remodel specific associations of mitochondria, lipid bodies, peroxisomes, and the endoplasmic reticulum. Hypothyroidism increases nuclear catalase immunopositivity and binuclearity in hepatocytes. Protection against lipid body deposition and steatosis is mediated by peroxisome biogenesis and maintenance of antioxidant defense.

- The importance of recognizing the metabolic and redox tissue-specific signature during methimazole administration and the significance of antioxidant intervention to mitigate early liver-specific changes in antioxidative defense are acknowledged.

- Although white AT does not change its structure in hypothyroidism, SAT and VAT depots respond in a distinct manner. SAT exhibits an early, division-driven increase in peroxisomes, while VAT depots respond later, using division followed by *de novo* biogenesis. This is accompanied by the appearance of pexopodium-like structures infiltrating lipid bodies at different time points, underlining distinct functional peroxisomal differences within VAT depots during hypothyroidism.

- The detected depot- and time-dependent variations in peroxisome appearance and formation may provide a potential explanation for the location-specific responses of adipocytes to hypothyroidism. This study expands current knowledge by revealing that white AT exhibits varied peroxisomal remodeling adaptations to hypothyroidism, rather than a uniform response. By identifying depot-specific structural and molecular adaptations of peroxisomes, this study proposes a novel conceptual model for interpreting how thyroid-related metabolic imbalances are driven by fat tissue heterogeneity.

The liver and WAT share substrates for lipid metabolism and store lipids as an energy reservoir. In conditions of TH deficiency, or hypothyroidism, the liver and WAT alter their organelles to prevent or mitigate pathological changes.

7. REFERENCE

Abeysekera KWM, Fernandes GS, Hammerton G, *et al.* Prevalence of steatosis and fibrosis in young adults in the UK: a population-based study. *Lancet Gastroenterol Hepatol*. 2020;5(3):295-305. doi:10.1016/S2468-1253(19)30419-4

Agrawal G, Subramani S. De novo peroxisome biogenesis: Evolving concepts and conundrums. *Biochim Biophys Acta*. 2016;1863(5):892-901. doi:10.1016/j.bbamcr.2015.09.014

Aleksic M, Golic I, Kalezic A, Jankovic A, Korac B, Korac A. Hypothyroidism Intensifies Both Canonic and the *De Novo* Pathway of Peroxisomal Biogenesis in Rat Brown Adipocytes in a Time-Dependent Manner. *Cells*. 2021;10(9):2248. doi:10.3390/cells10092248

Aleksic M, Kalezic A, Saso L, Jankovic A, Korac B, Korac A. The Unity of Redox and Structural Remodeling of Brown Adipose Tissue in Hypothyroidism. *Antioxidants (Basel)*. 2021;10(4):591. doi:10.3390/antiox10040591

Ayati Firoozabadi A, Elahi Vahed I, Lotfi P, Geshani A, Keshavarzian A, Moftakhar M, Razaghi M, Rasouli Z, Montazeri M, Mansournia MA, Vosough M, Rahmanian M. The reciprocal relationship between non-alcoholic fatty liver disease and hypothyroidism: A systematic review and meta-analysis of about 39 million individuals. *PLoS One*. 2025;20(12):e0338413. doi: 10.1371/journal.pone.0338413

Baskol G, Atmaca H, Tanriverdi F, Baskol M, Kocer D, Bayram F. Oxidative stress and enzymatic antioxidant status in patients with hypothyroidism before and after treatment. *Exp Clin Endocrinol Diabetes*. 2007;115(8):522-526. doi:10.1055/s-2007-981457

Beutler E. Catalase. In Red cell metabolism: a manual of biochemical methods (pp. 105–106). 1982. Grune and Stratton Inc.

Binns D, Januszewski T, Chen Y, *et al.* An intimate collaboration between peroxisomes and lipid bodies. *J Cell Biol*. 2006;173(5):719-731. doi:10.1083/jcb.200511125

Blanchette EJ. Ovarian steroid cells. II. The lutein cell. *J Cell Biol*. 1966;31(3):517-542. doi:10.1083/jcb.31.3.517

Bloom W, Fawcett DW: A Textbook of Histology, 10th ed. Philadelphia, Saunders, 1975.

Blouin A, Bolender RP, Weibel ER. Distribution of organelles and membranes between hepatocytes and nonhepatocytes in the rat liver parenchyma. A stereological study. *J Cell Biol*. 1977;72(2):441-455. doi:10.1083/jcb.72.2.441

Buzadzić B, Petrović V, Vasilijević A, Janković A, Korać B, Korać A. Alterations in L-arginine-nitric oxide-producing pathway affect antioxidative defense in the rat skin. *J Dermatol Sci*. 2007;47(1):41-44. doi:10.1016/j.jdermsci.2007.02.011

Čakić-Milošević M, Korać A, Davidović V. Methimazole-induced hypothyroidism in rats: effects on body weight and histological characteristics of thyroid gland. *Yugoslav Med Biochem*. 2004;23:143-147

Cano-Europa E, Blas-Valdivia V, Lopez-Galindo GE, *et al.* Methimazole-induced hypothyroidism causes alteration of the REDOX environment, oxidative stress, and hepatic damage; events not caused by hypothyroidism itself. *Ann Hepatol*. 2010;9(1):80-88.

Cano-Europa E, Blas-Valdivia V, Franco-Colin M, Gallardo-Casas CA, Ortiz-Butrón R. Methimazole-induced hypothyroidism causes cellular damage in the spleen, heart, liver, lung and kidney. *Acta Histochem*. 2011;113(1):1-5. doi:10.1016/j.acthis.2009.07.004

Carmichael RE, Richards DM, Fahimi HD, Schrader M. Organelle Membrane Extensions in Mammalian Cells. *Biology (Basel)*. 2023;12(5):664. doi:10.3390/biology12050664

Chung GE, Kim D, Kim W, *et al.* Non-alcoholic fatty liver disease across the spectrum of hypothyroidism. *J Hepatol*. 2012;57(1):150-156. doi:10.1016/j.jhep.2012.02.027

Cooper DS. Antithyroid drugs. *N Engl J Med*. 1984;311(21):1353-1362. doi:10.1056/NEJM198411223112106

da Rosa Araujo AS, Silva de Miranda MF, de Oliveira UO, *et al.* Increased resistance to hydrogen peroxide-induced cardiac contracture is associated with decreased myocardial oxidative stress in hypothyroid rats. *Cell Biochem Funct*. 2010;28(1):38-44. doi:10.1002/cbf.1616

Das K, Chainy GB. Modulation of rat liver mitochondrial antioxidant defence system by thyroid hormone. *Biochim Biophys Acta*. 2001;1537(1):1-13. doi:10.1016/s0925-4439(01)00048-5

Delille HK, Alves R, Schrader M. Biogenesis of peroxisomes and mitochondria: linked by division. *Histochem Cell Biol*. 2009;131(4):441-446. doi:10.1007/s00418-009-0561-9

Farré JC, Mahalingam SS, Proietto M, Subramani S. Peroxisome biogenesis, membrane contact sites, and quality control. *EMBO Rep*. 2019;20(1):e46864. doi:10.15252/embr.201846864

Fernández V, Barrientos X, Kipreos K, Valenzuela A, Videla LA. Superoxide radical generation, NADPH oxidase activity, and cytochrome P-450 content of rat liver microsomal fractions in an experimental hyperthyroid state: relation to lipid peroxidation. *Endocrinology*. 1985;117(2):496-501. doi:10.1210/endo-117-2-496

Gao Q, Goodman JM. The lipid droplet-a well-connected organelle. *Front Cell Dev Biol*. 2015;3:49. doi:10.3389/fcell.2015.00049

Gariani K, Jornayvaz FR. Pathophysiology of NASH in endocrine diseases. *Endocr Connect*. 2021;10(2):R52-R65. doi:10.1530/EC-20-0490

Gebhardt R, Matz-Soja M. Liver zonation: Novel aspects of its regulation and its impact on homeostasis. *World J Gastroenterol*. 2014;20(26):8491-8504. doi:10.3748/wjg.v20.i26.8491

Glatzle D, Vuilleumier JP, Weber F, Decker K. Glutathione reductase test with whole blood, a convenient procedure for the assessment of the riboflavin status in humans. *Experientia*. 1974;30(6):665-667. doi:10.1007/BF01921531

Goldberg AA, Bourque SD, Kyryakov P, *et al.* A novel function of lipid droplets in regulating longevity. *Biochem Soc Trans*. 2009;37(Pt 5):1050-1055. doi:10.1042/BST0371050

Goto T, Lee JY, Teraminami A, *et al.* Activation of peroxisome proliferator-activated receptor-alpha stimulates both differentiation and fatty acid oxidation in adipocytes. *J Lipid Res*. 2011;52(5):873-884. doi:10.1194/jlr.M011320

Griffith OW. Determination of glutathione and glutathione disulfide using glutathione reductase and 2-vinylpyridine. *Anal Biochem*. 1980;106(1):207-212. doi:10.1016/0003-2697(80)90139-6

Guerrero A, Pamplona R, Portero-Otín M, Barja G, López-Torres M. Effect of thyroid status on lipid composition and peroxidation in the mouse liver. *Free Radic Biol Med*. 1999;26(1-2):73-80. doi:10.1016/s0891-5849(98)00173-7

Habig WH, Pabst MJ, Jakoby WB. Glutathione S-transferases. The first enzymatic step in mercapturic acid formation. *J Biol Chem*. 1974;249(22):7130-7139.

Harper ME, Brand MD. Hyperthyroidism stimulates mitochondrial proton leak and ATP turnover in rat hepatocytes but does not change the overall kinetics of substrate oxidation reactions. *Can J Physiol Pharmacol*. 1994;72(8):899-908. doi:10.1139/y94-127

Hebel R, Stromberg MW. Digestive system. In: Hebel R, Stromberg MW, (eds). Anatomy of the Laboratory Rat. Baltimore: Williams and Wilkins Co.; 1986. pp. 46–57

Hollander CF, de Leeuw AM, van Zwieten MJ. Embryology, Anatomy, Histology, and Ultrastructure of the Liver, Rat. In: Jones TC, Mohr U, Hunt RD. (eds) Digestive System. Monographs on Pathology of Laboratory Animals. Springer, Berlin, Heidelberg. 1985. https://doi.org/10.1007/978-3-642-96910-2_1

Horrum MA, Tobin RB, Ecklund RE. Thyroxine-induced changes in rat liver mitochondrial cytochromes. *Mol Cell Endocrinol*. 1985;41(2-3):163-169. doi:10.1016/0303-7207(85)90019-x

Janković A, Buzadžić B, Korać A, *et al.* Antioxidative defense organization in retroperitoneal white adipose tissue during acclimation to cold – the involvement of L-arginine/NO pathway. *J Therm Biol* 2009; 34:358-365.

Jomova K, Raptova R, Alomar SY, *et al.* Reactive oxygen species, toxicity, oxidative stress, and antioxidants: chronic diseases and aging. *Arch Toxicol*. 2023;97(10):2499-2574. doi:10.1007/s00204-023-03562-9

Jones JM, Morrell JC, Gould SJ. PEX19 is a predominantly cytosolic chaperone and import receptor for class 1 peroxisomal membrane proteins. *J Cell Biol*. 2004;164(1):57-67. doi:10.1083/jcb.200304111

Karperien A. FracLac for ImageJ. Published 2013. Accessed [October 29, 2025]. https://imagej.net/ij/plugins/fraclac/FLHelp/Introduction.htm

Koch A, Yoon Y, Bonekamp NA, McNiven MA, Schrader M. A role for Fis1 in both mitochondrial and peroxisomal fission in mammalian cells. *Mol Biol Cell*. 2005;16(11):5077-5086. doi:10.1091/mbc.e05-02-0159

Koch J, Pranjic K, Huber A, *et al.* PEX11 family members are membrane elongation factors that coordinate peroxisome proliferation and maintenance. *J Cell Sci*. 2010;123(Pt 19):3389-3400. doi:10.1242/jcs.064907

Kochman J, Jakubczyk K, Bargiel P, Janda-Milczarek K. The Influence of Oxidative Stress on Thyroid Diseases. *Antioxidants (Basel)*. 2021;10(9):1442. Published 2021 Sep 10. doi:10.3390/antiox10091442

Kunze M, Pracharoenwattana I, Smith SM, Hartig A. A central role for the peroxisomal membrane in glyoxylate cycle function. *Biochim Biophys Acta*. 2006;1763(12):1441-1452. doi:10.1016/j.bbamcr.2006.09.009

Lazo-de-la-Vega-Monroy ML, Preciado-Puga MD, Ruiz-Noa Y, Salum-Zertuche M, Ibarra-Reynoso LD. Correlation of the pediatric metabolic index with NAFLD or MAFLD diagnosis, and serum adipokine levels in children. *Clin Res Hepatol Gastroenterol*. 2023;47(6):102137. doi:10.1016/j.clinre.2023.102137

LeHir M, Herzog V, Fahimi HD. Cytochemical detection of catalase with 3,3'-diaminobenzidine. A quantitative reinvestigation of the optimal conditions. *Histochemistry*. 1979;64(1):51-66. doi:10.1007/BF00493354

Li X, Gould SJ. PEX11 promotes peroxisome division independently of peroxisome metabolism. *J Cell Biol*. 2002;156(4):643-651. doi:10.1083/jcb.200112028

Liu Y, Wang W, Yu X, Qi X. Thyroid Function and Risk of Non-Alcoholic Fatty Liver Disease in Euthyroid Subjects. *Ann Hepatol*. 2018;17(5):779-788. doi:10.5604/01.3001.0012.3136

Lowry OH, Rosebrough NJ, Farr AL, Randall RJ. Protein measurement with the Folin phenol reagent. *J Biol Chem*. 1951;193(1):265-275. doi.10.1016/s0021-9258(19)52451-6

Luthman M, Holmgren A. Rat liver thioredoxin and thioredoxin reductase: purification and characterization. *Biochemistry*. 1982;21(26):6628-6633. doi:10.1021/bi00269a003

Mason RL, Hunt HM, Hurxthal L. Blood cholesterol values in hyperthyroidism and hypothyroidism — their significance. *N Engl J Med*. 1930;203:1273-1278

Misra HP, Fridovich I. The role of superoxide anion in the autoxidation of epinephrine and a simple assay for superoxide dismutase. *J Biol Chem*. 1972;247(10):3170-3175.

Mutvei A, Nelson BD. The response of individual polypeptides of the mammalian respiratory chain to thyroid hormone. *Arch Biochem Biophys*. 1989;268(1):215-220. doi:10.1016/0003-9861(89)90582-1

Olzmann JA, Carvalho P. Dynamics and functions of lipid droplets. *Nat Rev Mol Cell Biol*. 2019;20(3):137-155. doi:10.1038/s41580-018-0085-z

Oren R, Dotan I, Papa M, *et al.* Inhibition of experimentally induced cirrhosis in rats by hypothyroidism. *Hepatology*. 1996;24(2):419-423. doi:10.1053/jhep.1996.v24.pm0008690414

Paglia DE, Valentine WN. Studies on the quantitative and qualitative characterization of erythrocyte glutathione peroxidase. *J Lab Clin Med*. 1967;70(1):158-169.

Park H, He A, Tan M, *et al.* Peroxisome-derived lipids regulate adipose thermogenesis by mediating cold-induced mitochondrial fission. *J Clin Invest*. 2019;129(2):694-711. doi:10.1172/JCI120606

Pearce EN. Update in lipid alterations in subclinical hypothyroidism. *J Clin Endocrinol Metab*. 2012;97(2):326-333. doi:10.1210/jc.2011-2532

Pu S, Zhao B, Jiang Y, Cui X. Hypothyroidism/subclinical hypothyroidism and metabolic dysfunction-associated steatotic liver disease: advances in mechanism and treatment. *Lipids Health Dis*. 2025;24(1):75. doi:10.1186/s12944-025-02474-0

Pucci E, Chiovato L, Pinchera A. Thyroid and lipid metabolism. *Int J Obes Relat Metab Disord*. 2000;24 Suppl 2:S109-S112. doi:10.1038/sj.ijo.0801292

Ramanathan R, Patwa SA, Ali AH, Ibdah JA. Thyroid Hormone and Mitochondrial Dysfunction: Therapeutic Implications for Metabolic Dysfunction-Associated Steatotic Liver Disease (MASLD). *Cells*. 2023;12(24):2806. doi:10.3390/cells12242806

Rollins DE, Blumenthal DK. Thyroid and antithyroid drugs. In: Workbook and Casebook for Goodman and Gilman's The Pharmacological Basis of Therapeutics, 2016, 1383-1409.

Sahoo DK, Roy A, Bhanja S, Chainy GB. Hypothyroidism impairs antioxidant defence system and testicular physiology during development and maturation. *Gen Comp Endocrinol*. 2008;156(1):63-70. doi:10.1016/j.ygcen.2007.11.007

Scholz P, Chapman KD, Mullen RT, Ischebeck T. Finding new friends and revisiting old ones - how plant lipid droplets connect with other subcellular structures. *New Phytol*. 2022;236(3):833-838. doi:10.1111/nph.18390

Schrader M, Reuber BE, Morrell JC, *et al.* Expression of PEX11beta mediates peroxisome proliferation in the absence of extracellular stimuli. *J Biol Chem*. 1998;273(45):29607-29614. doi:10.1074/jbc.273.45.29607

Schrader M. Tubulo-reticular clusters of peroxisomes in living COS-7 cells: dynamic behavior and association with lipid droplets. *J Histochem Cytochem*. 2001;49(11):1421-1429. doi:10.1177/002215540104901110

Seifert J, Chen Y, Schöning W, *et al.* Hepatic Energy Metabolism under the Local Control of the Thyroid Hormone System. *Int J Mol Sci*. 2023;24(5):4861. doi:10.3390/ijms24054861

Sinha RA, Singh BK, Yen PM. Direct effects of thyroid hormones on hepatic lipid metabolism. *Nat Rev Endocrinol*. 2018;14(5):259-269. doi:10.1038/nrendo.2018.10

Soares De Oliveira L, Ritter MJ. Thyroid hormone and the Liver. *Hepatol Commun*. 2024;9(1):e0596. doi:10.1097/HC9.0000000000000596

Tanase DM, Gosav EM, Neculae E, *et al.* Hypothyroidism-Induced Nonalcoholic Fatty Liver Disease (HIN): Mechanisms and Emerging Therapeutic Options. *Int J Mol Sci*. 2020;21(16):5927. doi:10.3390/ijms21165927

Thazar-Poulot N, Miquel M, Fobis-Loisy I, Gaude T. Peroxisome extensions deliver the Arabidopsis SDP1 lipase to oil bodies. *Proc Natl Acad Sci U S A.* 2015;112(13):4158-4163. doi:10.1073/pnas.1403322112

Thoms S, Erdmann R. Dynamin-related proteins and Pex11 proteins in peroxisome division and proliferation. *FEBS J*. 2005;272(20):5169-5181. doi:10.1111/j.1742-4658.2005.04939.x

Trayhurn P, Beattie JH. Physiological role of adipose tissue: white adipose tissue as an endocrine and secretory organ. *Proc Nutr Soc*. 2001;60(3):329-339. doi:10.1079/pns200194

Vdoviaková K, Vdoviaková K, Petrovová E, *et al.* Importance Rat Liver Morphology and Vasculature in Surgical Research. *Med Sci Monit*. 2016;22:4716-4728. doi:10.12659/msm.899129

Venditti P, Balestrieri M, Di Meo S, De Leo T. Effect of thyroid state on lipid peroxidation, antioxidant defences, and susceptibility to oxidative stress in rat tissues. *J Endocrinol*. 1997;155(1):151-157. doi:10.1677/joe.0.1550151

Vidal-Cevallos P, Murúa-Beltrán Gall S, Uribe M, Chávez-Tapia NC. Understanding the Relationship between Nonalcoholic Fatty Liver Disease and Thyroid Disease. *Int J Mol Sci*. 2023;24(19):14605. Published 2023 Sep 27. doi:10.3390/ijms241914605.

Walther TC, Farese RV Jr. Lipid droplets and cellular lipid metabolism. *Annu Rev Biochem*. 2012;81:687-714. doi:10.1146/annurev-biochem-061009-102430

Wang S, Xia D, Fan H, *et al.* Low thyroid function is associated with metabolic dysfunction-associated steatotic liver disease. *JGH Open*. 2024;8(2):e13038. doi:10.1002/jgh3.13038

Welte MA. Expanding roles for lipid droplets. *Curr Biol*. 2015;25(11):R470-R481. doi:10.1016/j.cub.2015.04.004

Yorke E. Co-Morbid Hypothyroidism and Liver Dysfunction: A Review. *Clin Med Insights Endocrinol Diabetes*. 2024;17:11795514241231533. doi:10.1177/11795514241231533

Zuarth-Vázquez J, Moreno-Castañeda L, Soriano-Márquez JP, *et al.* Low-Normal Thyroid Function Is Not Associated with Either Non-Alcoholic Fatty Liver Disease or with Metabolic Dysfunction-Associated Fatty Liver Disease. *Life (Basel)*. 2023;13(4):1048. Published 2023 Apr 19. doi:10.3390/life13041048

BIOGRAPHY

Ahsein Mohamed. A. Addloli was born in Sabha, Libya, on May 02 1984. He started his Bachelor studies in 2003-2004 at the Faculty of Science, Biology department, At Bani Waleed University, where he graduated on 2006-2007.

From 2007-2010 Ahsein Mohamed. A. Addloli worked as a Demonstrator in biology department at Bani Waleed University, where he taught the following courses: Physiology, Genetics, Histology, Immunology, General zoology.

In 2011 he enrolled in master studies at the Faculty of Biology, University of Belgrade study program Biology, module Cell and Tissue Biology and he graduated on 2014.
In 2015 he enrolled in doctoral studies at the Faculty of Biology, University of Belgrade, study program Biology, module Cell and Tissue Biology.

He has published works independently or as a co-author in prominent international journals, in addition to participating in international conferences. His work contributes to enhancing the understanding of oxidative stress and endocrine disorders through experimental biological research.

Изјава о ауторству

Име и презиме аутора Ahsein Addloli

Број индекса Б3042/2015

Изјављујем

да је докторска дисертација под насловом

Структурно и редокс ремоделирање јетре и белог масног ткива пацова у хипотироидизму изазваном метимазолом / Structural and redox remodeling of the liver and white adipose tissue of rats in methimazole-induced hypothyroidism

- резултат сопственог истраживачког рада;
- да дисертација у целини ни у деловима није била предложена за стицање друге дипломе према студијским програмима других високошколских установа;
- да су резултати коректно наведени и
- да нисам кршио/ла ауторска права и користио/ла интелектуалну својину других лица.

Потпис аутора

У Београду, 05.08.2026.год.

Изјава о истоветности штампане и електронске верзије докторског рада

Име и презиме аутора Ahsein Addloli

Број индекса Б3042/2015

Студијски програм Биологија, модул Биологија ћелија и ткива

Наслов рада Структурно и редокс ремоделирање јетре и белог масног ткива пацова у хипотироидизму изазваном метимазолом / Structural and redox remodeling of the liver and white adipose tissue of rats in methimazole-induced hypothyroidism

Ментори др Александра Корач, редовни професор Универзитет у Београду-Биолошки факултет

др Бато Корач, научни саветник, Универзитет у Бегораду-Институт за биолошка истраживања „Синиша Станковић"-Институт од националног значаја за Републику Србију

Изјављујем да је штампана верзија мог докторског рада истоветна електронској верзији коју сам предао/ла ради похрањивања у **Дигиталном репозиторијуму Универзитета у Београду.**

Дозвољавам да се објаве моји лични подаци везани за добијање академског назива доктора наука, као што су име и презиме, година и место рођења и датум одбране рада.

Ови лични подаци могу се објавити на мрежним страницама дигиталне библиотеке, у електронском каталогу и у публикацијама Универзитета у Београду.

Потпис аутора

У Београду, 05.08.2026. год.

Изјава о коришћењу

Овлашћујем Универзитетску библиотеку „Светозар Марковић“ да у Дигитални репозиторијум Универзитета у Београду унесе моју докторску дисертацију под насловом:

Структурно и редокс ремоделирање јетре и белог масног ткива пацова у хипотироидизму изазваном метимазолом / Structural and redox remodeling of the liver and white adipose tissue of rats in methimazole-induced hypothyroidism

која је моје ауторско дело.

Дисертацију са свим прилозима предао/ла сам у електронском формату погодном за трајно архивирање.

Моју докторску дисертацију похрањену у Дигиталном репозиторијуму Универзитета у Београду и доступну у отвореном приступу могу да користе сви који поштују одредбе садржане у одабраном типу лиценце Креативне заједнице (Creative Commons) за коју сам се одлучио/ла.

1. Ауторство (CC BY)

2. Ауторство – некомерцијално (CC BY-NC)

3. Ауторство – некомерцијално – без прерада (CC BY-NC-ND)

4. Ауторство – некомерцијално – делити под истим условима (CC BY-NC-SA)

5. Ауторство – без прерада (CC BY-ND)

6. Ауторство – делити под истим условима (CC BY-SA)

(Молимо да заокружите само једну од шест понуђених лиценци. Кратак опис лиценци је саставни део ове изјаве).

Потпис аутора

У Београду, 05.08.2026. год.

1. **Ауторство**. Дозвољавате умножавање, дистрибуцију и јавно саопштавање дела, и прераде, ако се наведе име аутора на начин одређен од стране аутора или даваоца лиценце, чак и у комерцијалне сврхе. Ово је најслободнија од свих лиценци.

2. **Ауторство – некомерцијално**. Дозвољавате умножавање, дистрибуцију и јавно саопштавање дела, и прераде, ако се наведе име аутора на начин одређен од стране аутора или даваоца лиценце. Ова лиценца не дозвољава комерцијалну употребу дела.

3. **Ауторство – некомерцијално – без прерада**. Дозвољавате умножавање, дистрибуцију и јавно саопштавање дела, без промена, преобликовања или употребе дела у свом делу, ако се наведе име аутора на начин одређен од стране аутора или даваоца лиценце. Ова лиценца не дозвољава комерцијалну употребу дела. У односу на све остале лиценце, овом лиценцом се ограничава највећи обим права коришћења дела.

4. **Ауторство – некомерцијално – делити под истим условима**. Дозвољавате умножавање, дистрибуцију и јавно саопштавање дела, и прераде, ако се наведе име аутора на начин одређен од стране аутора или даваоца лиценце и ако се прерада дистрибуира под истом или сличном лиценцом. Ова лиценца не дозвољава комерцијалну употребу дела и прерада.

5. **Ауторство – без прерада**. Дозвољавате умножавање, дистрибуцију и јавно саопштавање дела, без промена, преобликовања или употребе дела у свом делу, ако се наведе име аутора на начин одређен од стране аутора или даваоца лиценце. Ова лиценца дозвољава комерцијалну употребу дела.

6. **Ауторство – делити под истим условима**. Дозвољавате умножавање, дистрибуцију и јавно саопштавање дела, и прераде, ако се наведе име аутора на начин одређен од стране аутора или даваоца лиценце и ако се прерада дистрибуира под истом или сличном лиценцом. Ова лиценца дозвољава комерцијалну употребу дела и прерада. Слична је софтверским лиценцама, односно лиценцама отвореног кода.